Contribution of K_v2.1 channels to the delayed rectifier current in freshly dispersed smooth muscle cells from rabbit urethra

B. Kyle[1], E. Bradley[1], S. Ohya[2], G. P. Sergeant[1], N. G. McHale[1], K. D. Thornbury[1] & M.A Hollywood[1]

[1]The Smooth Muscle Research Centre, Dundalk Institute of Technology, Dublin Road, Dundalk, Co. Louth, Ireland & [2]Molecular & Cellular Pharmacology, Graduate School of Pharmaceutical Sciences, Nagoya City University, Nagoya, Japan.

Name and address for correspondence:

Mark Hollywood
Smooth Muscle Research Centre
Dundalk Institute of Technology
Dublin Road
Dundalk
Ireland

Tel: (00353) 429370475
Fax: (00353) 429370509
Email: mark.hollywood@dkit.ie
Web: www.smoothmusclegroup.org

Key words: urethra, delayed rectifier current, Kv2.1, Kv2.2, smooth muscle

ABSTRACT

We have characterized the native voltage-dependent K^+ (K_v) current in rabbit urethral smooth muscle cells (RUSMC) and compared its pharmacological and biophysical properties with $K_v2.1$ and $K_v2.2$ channels cloned from the rabbit urethra and stably expressed in HEK 293 cells ($HEK_{Kv2.1}$ and $HEK_{Kv2.2}$). RUSMC were perfused with Hanks' solution at 37°C and studied using the patch clamp technique with K^+-rich pipette solutions. Cells were bathed in 100 nM penitrem A (Pen A) to block large conductance Ca^{2+}-activated K^+ (BK) currents and depolarized to +40 mV for 500 ms to evoke K_v currents. These were unaffected by margatoxin, κ-dendrotoxin or α-dendrotoxin (100 nM, n=3-5), but were blocked by stromatoxin-1 (ScTx, IC_{50}~130 nM), consistent with the idea that the currents were carried through K_v2 channels. RNA was detected for $K_v2.1$ $K_v2.2$ and the silent subunit $K_v9.3$ in urethral smooth muscle. Immunocytochemistry showed membrane staining for both K_v2 subtypes and $K_v9.3$ in isolated RUSMC. $HEK_{Kv2.1}$ and $HEK_{Kv2.2}$ currents were blocked in a concentration dependent manner by ScTx with estimated IC_{50} values of ~150 nM ($K_v2.1$, n=5) and 70 nM ($K_v2.2$, n=6). The mean $V_{1/2}$ of inactivation of the USMC K_v current was –56±3 mV (n=9). This was similar to the $HEK_{Kv2.1}$ current (–55 ± 3 mV, n=13) but significantly different from the $HEK_{Kv2.2}$ currents (-30 ± 3 mV, n=11). Action potentials (AP) evoked from RUSMC studied under current clamp mode were unaffected by ScTx. However when ScTx was applied in the presence of Pen A, the AP duration was significantly prolonged. Similarly, ScTx increased the amplitude of spontaneous contractions threefold, but only after Pen A application.

These data suggest that $K_v2.1$ channels contribute significantly to the K_v current in RUSMC.

73 **INTRODUCTION**

74

75 The urethra plays an important role in the maintenance of urinary continence by generating
76 sufficient force to prevent urine outflow from the bladder. The spontaneous activity in the
77 urethra is thought to be initiated and modulated by specialised pacemaking cells, which
78 control the bulk smooth muscle (33). Although a number of studies have characterised the
79 main inward currents in urethral smooth muscle and assessed their role in urethral tone (6, 9,
80 18), little is known about the voltage gated K^+ (K_v) currents in these cells. The majority of
81 work on urethral K^+ currents has focused on examining the role of K_{ATP} channels in isolated
82 pig myocytes (34, 35, 36). The contribution of other K^+ channels to the electrical activity in
83 the urethra is poorly understood and few studies have focused on examining which K_v
84 subtypes are present (5). Hollywood *et al.* (2000) unmasked an iberiotoxin- and Pen A-
85 insensitive K_v current, which was TEA-sensitive and contributed to the repolarisation phase
86 of evoked action potentials. However, the molecular identity of the K_v channels underlying
87 the K_v current in urethra remain undetermined.
88 The molecular identity of K_v channels in the bladder (7, 24, 37) has been examined in more
89 detail and it has been demonstrated that K_v2 expression is significantly higher than K_v1 in the
90 rat bladder (24). Similarly, Thornloe & Nelson (2003) found that the delayed rectifier
91 currents in murine urinary bladder cells were likely to be carried through $K_v2.1$ channels. It is
92 likely that these channels help regulate contractions in the bladder since, blockade of K_v2
93 channels with stromatoxin-1 (ScTx) enhances both myogenic and neurogenic contractions in
94 the rat bladder (7).
95 Given that K_v2 channels appear to play an important role in bladder smooth muscle, we have
96 examined if they also contribute to the delayed rectifier in urethral smooth muscle. In this
97 paper, the molecular identity and cellular expression of the K_v current present in RUSMCs is
98 examined and the biophysical, pharmacological and functional properties of the K_v current
99 are investigated. The results demonstrate that isolated RUSMC are immunopositive for K_v2
100 channels and a ScTx sensitive K_v2 channel is likely to carry the K_v current in freshly
101 dispersed rabbit urethral myocytes. Furthermore a comparison of the native current with
102 $K_v2.1$ and $K_v2.2$ cloned from the rabbit urethra and stably expressed in HEK 293 cells
103 suggests that the native current shares a number of features consistent with it being $K_v2.1$.
104 These data suggest that although K_v2 channels can modify electrical activity and myogenic
105 contractions, they only play a significant role when BK currents are inhibited.

106

107 **Materials and Methods**

108 All procedures were carried out in accordance with current EU legislation and with the
109 approval of Dundalk Institute of Technology Animal Care and Use Committee. Male and
110 female New Zealand white rabbits (16-20 weeks old) were humanely killed with a lethal
111 injection of pentobarbitone (i.v.)

112

113 **Cell Isolation**

114 The most proximal 1.5 cm of the urethra was removed and placed in Krebs solution. Strips of
115 proximal urethra, 0.5 cm in width were cut into 1 mm^3 pieces and stored in Hanks Ca^{2+} free
116 solution for 30 min before being incubated in dispersal medium containing (per 5mls of Ca^{2+}-
117 free Hanks solution (see solutions)): 15mg collagenase (Sigma type 1A), 0.5mg protease
118 (Sigma type XXIV), 5mg bovine serum albumin (Sigma) and 15mg trypsin inhibitor (Sigma)
119 for 10-15 mins at 37˚C. Tissue was then transferred to Ca^{2+}-free Hanks solution and stirred
120 for a further 15-30 min to release single smooth muscle cells. These cells were plated in petri
121 dishes containing 100 µM Ca^{2+} Hank's solution and stored at 4˚C for use within 8 hours.

122

123 **Patch Clamp Recordings**

124 Currents from RUSMC were recorded with the perforated patch configuration of the whole
125 cell patch clamp technique (28). The cell membrane was perforated using the antibiotic
126 amphotericin B (600µg/ml). Patch pipettes were initially front-filled by dipping into pipette
127 solution and then back filled with the amphotericin B containing solution. For experiments
128 on HEK293 cells, currents were recorded using the ruptured patch configuration of the patch
129 clamp technique (13). Pipettes were pulled from borosilicate glass capillary tubing (1.5mm
130 outer diameter, 1.17mm inner diameter; Clark Medical Instruments) to a tip of diameter
131 approximately 1-1.5µm and resistance of 2-4MΩ.

132 Series resistance and capacitative currents were usually compensated by up to 80% in this
133 study. Voltage clamp commands were delivered via an Axopatch 1D patch clamp amplifier
134 (Axon Instruments) connected to a Digidata 1322A AD/DA converter (Axon Instruments)
135 interfaced to a computer running pClamp software (Axon Instruments).

136

137 **Solutions**

138 The composition of the solutions used was as follows (in mM): *Hanks solution:* 129.8 Na^+,
139 5.8 K^+, 135 Cl^-, 4.17 HCO_3^- 0.34 HPO_4^{2-}, 0.44 $H_2PO_4^-$, 1.8 Ca^{2+}, 0.9 Mg^{2+}, 0.4 SO_4^{2-}, 10
140 glucose, 2.9 sucrose and 10 HEPES, pH adjusted to 7.4 with NaOH. *Ca^{2+} free Hanks*
141 *perfusate solution:* 129.8 Na^+, 5.8 K^+, 135 Cl^-, 4.17 HCO_3^-, 0.34 HPO_4^{2-}, 0.44 $H_2PO_4^-$, 2.7
142 Mg^{2+}, 0.4 SO_4^{2-}, 10 glucose, 2.9 sucrose, 5 EGTA and 10 HEPES, pH adjusted to 7.4 with
143 NaOH. *Ca^{2+} free Hanks cell dispersal solution:* NaCl (125), KCl (5.36), glucose (10),
144 sucrose (2.9), $NaHCO_3$ (15.5), KH_2PO_4 (0.44), Na_2HPO_4 (0.33), N-[2-
145 Hydroxyethylpiperazine]-N'-[2-ethanesulfonic acid] (HEPES; 10) pH adjusted to 7.4 with
146 NaOH. *Krebs solution:* NaCl (120), KCl (5.9), $NaHCO_3$ (1.2), glucose (5.5) $CaCl_2$ (12.5),
147 $MgCl_2$ (6) pH maintained at 7.4 by bubbling with 95% O_2-5% CO_2. *K^+ pipette solution*
148 (whole cell)*:* 132 K^+, 110 gluconate, 21 Cl^-, 2 Na^+, 0.5 Mg^{2+}, 1 ATP, 0.1 GTP, 2.5
149 phosphocreatine, 5 HEPES and 1 EGTA; pH adjusted to 7.2 with KOH. *K^+ pipette solution*
150 (perforated patch): 133 K^+, 135 Cl^-, 1 Mg^{2+}, 0.5 EGTA and 10 HEPES; pH adjusted to 7.2
151 with KOH.

152 During experiments, the dish containing the cells was superfused with Hanks solution. In
153 addition, the cell under study was continuously superfused with Hanks solution by means of
154 a close delivery system consisting of a pipette (tip diameter 200 µm) placed approximately
155 300 µm away. This could be switched, with a dead-space time of around five seconds, to a
156 solution containing a drug. All experiments were carried out at 36±1°C.

157

158 **Statistics**

159 Experiments on freshly dispersed RUSMCs were usually carried out on a minimum of 3
160 animals. In all experiments 'n' refers to the number of cells studied. Summary data are
161 presented as the mean ± S.E.M and statistical comparisons were made on raw data using
162 students paired *t*-test, unpaired t-test or ANOVA as appropriate, taking $p<0.05$ level as
163 significant. In the Figures * represents $p<0.05$, ** represents $p<0.01$ and *** represents
164 $p<0.001$.

165

166 **Total RNA isolation and RT-PCR**

167 Total RNA was prepared from brain and urethral smooth muscle strips using the TRIZOL
168 method (Invitrogen) as per manufacturers instructions and treated with DNase (Stratagene).

169 First strand cDNA was prepared from the RNA preparations using the Superscript II RNase
170 H reverse transcriptase (Invitrogen); 200 μg ml^{-1} of random hexamer was used to reverse
171 transcribe the RNA sample. The cDNA formed from the reverse transcription reaction was
172 amplified with specific primers by RT-PCR. This was preformed in a 25 μl reaction
173 containing 12.5 μl Amplitaq Gold Mastermix (Applied Biosystems), 8.5 μl of water, 1 μl of
174 sense and antisense primers (at a concentration of 10 μM) and 2 μl of template cDNA. All
175 reactions were performed in a Techne TC-512 gradient thermal cycler. The amplification
176 profile for all primer pairs were as follows: 95°C for 5 min, followed by 35 cycles of 95°C for
177 30 s and 56°C for 1 min, 72°C for 1 min, with a final extension step at 72°C for 7 min. The
178 amplified products were separated by electrophoresis on a 2% agarose–1 x TAE (Tris, acetic
179 acid, EDTA) gel and the DNA bands were subsequently visualized by ethidium bromide
180 staining and documented on an INGENIUS gel documentation system (Syngene Bio
181 Imaging).
182
183 **Quantitative Real-Time PCR**
184 Quantitative Real-Time RT-PCR (qPCR) was performed in a 25 μl reaction containing 12.5
185 μl SYBR Green Mastermix (Applied Biosystems), 8.5 μl of water, 1 μl of sense and antisense
186 primers (at a concentration of 10 μM) and 2 μl of template cDNA. The reaction was carried
187 out using a Techne – Quantica Real Time Thermal Cycler. The thermal protocol for the
188 qPCR was identical to that described above. We used the relative quantification method (3),
189 using the housekeeper gene, β-actin as an internal standard. Only primers with 90-110%
190 efficiency were used for these experiments, however differential primer efficiencies were
191 accounted for in this analysis by generation of standard curves (range 1:2 – 1:100 dilution).
192 Standard curves were generated for *Kv* subunit and β-actin mRNA from regression analysis
193 of the mean values of RT-PCRs for the log_{10} diluted cDNA. Unknown quantities relative to
194 the standard curve for the *Kv* primers were calculated, yielding transcriptional quantification
195 of *Kv* cDNA relative to β-actin. Each cDNA sample was tested in triplicate and cDNA was
196 obtained from a minimum of three different animals. Mean values generated at individual
197 time points were compared by ANOVA and statistical analyses were performed using
198 GraphPad Prism version 4 (GraphPad Software, San Diego, CA, USA). In order to validate
199 that the double stranded DNA fluorescence was primarily amplicon-based (as opposed to
200 primer dimer), melting curve analysis was employed by ramping the temperature from 70 °C

201 to 90 °C which resulting in melting of the double stranded DNA. If one distinct peak was
202 present, this was consistent with one PCR product resulting from the reaction.
203
204 **Primer design**
205 All primers for PCR were designed against the published rabbit sequence except for $K_v1.7$,
206 which was designed against the human sequence. In each case the number in parentheses
207 represents the GenBank accession number.
208
209 *Kv1.2* (NM_001082722.1):
210 sense nucleotide nt 168-183, GCAGCTGGAAGGCGTA
211 antisense nt 584-568, TCTCCATGGCCTCCTCA.
212 Amplicon, 417 base pairs (bp).
213
214 *Kv1.3* (NM_001171129.1):
215 sense nucleotide nt 343-358, AACGTGCCCATCGACA.
216 antisensent 740-756, GAGCAGCTCGAAGGAGA.
217 Amplicon 414 bp.
218
219 *Kv1.7* (AY779768.1):
220 sense nucleotide nt 637-659, TGCCCTTCAATGACCCGTTCTTC.
221 antisense nt 886-864, AAGACACGCACCAATCGGATGAC.
222 Amplicon 250 bp.
223
224 *Kv2.1* (NM_001082087.1):
225 sense nt 1060-1079, GTCCAGATCTTCCGCATCAT.
226 antisense nt 1255-1236, ACTTGGTGTCGTCCTCATCC.
227 Amplicon, 196 bp.
228
229 *Kv2.2* (NM_001082137.1):
230 sense nt 1561-1580, CGAAGTATGGAACTGATCGA.
231 antisense nt 1726-1707, CCTCCTGGTACTTATTCTCA.
232 Amplicon, 166 bp.
233

234 *Kv4.2* (NM_001082118.1):
235 sense nt 546-565, CATGGCCCTGGTGTTCTACT.
236 antisense nt 738-719, CAGCAAGTACTCGACGGTGA.
237 Amplicon 193 bp.
238
239 *Kv4.3* (NM_001082717.1):
240 sense nt 1573-1592, ATGCAGAACTACCCGTCCAC.
241 antisense nt 1783-1764, GATTAAGGCTGGAGCGACTG.
242 Amplicon 211 bp.
243
244 K_V*5.1* (XM_002722391):
245 sense nucleotide (nt) 732-750, 5'-GCCCAACAAGCTGCACTTC-3'
246 antisense nt 854-834, 5'-ACGTTGGTCAGCTCCATCATG-3'.
247 Amplicon, 123 bp.
248
249 K_V*6.1* (XM_002722694):
250 sense nucleotide (nt) 272-290, 5'-AGCTCAAGGCCTGCACCAA-3'
251 antisense nt 362-344, 5'-GGGTTGCGGTCGAAGAAGA-3'.
252 Amplicon, 111 bp.
253
254 K_V*6.3* (XM_002709903):
255 sense nucleotide (nt) 799-820, 5'-ATCTCCGTGCTGATGACAGTGT-3'
256 antisense nt 919-900, 5'-TGAAGTGACGGGCAAGCTTA-3'.
257 Amplicon, 121 bp.
258 K_V*9.1* (XM_002721207):
259 sense nucleotide (nt) 1025-1043, 5'-TCTCCGGTGTGGCCTACAC-3'
260 antisense nt 1135-1117, 5'-CATCCCCGTAGCCCACTGT-3'.
261 Amplicon, 111 bp.
262
263 K_V*9.2* (XM_002710709):
264 sense nucleotide (nt) 596-617, 5'-GCTCCATCATCACCATGTGTCT-3'
265 antisense nt 714-694, 5'-GAACCAGGCTATGCCAAAGTG-3'.
266 Amplicon, 119 bp.

267

268 *K_V9.3* (NM_001082652): sense nucleotide (nt) 796-817,

269 5'-TTCTATGCCACGTTGGCAGTAG-3'

270 antisense nt 916-897, 5'-GCCGGGCAAGCTTTAGAATT-3'.

271 Amplicon, 121 bp.

272

273 β-actin (AF404278),

274 sense nucleotide (nt) 1-20, 5'-GATTCACCATGGATGATGAT-3',

275 antisense nt 238-219, 5'-ACTAGTGATTGCTGCTCGAT-3'.

276 Amplicon. 238 bp

277

278 **HEK293 stable transfection with K_V2.1 and K_V2.2**

279 Total RNAs were extracted from homogenates of male New Zealand white rabbit urethra (16
280 weeks old) using the acid guanidium thiocyanate-phenol method, followed by digestion with
281 RNase-free DNase. Reverse-transcription was performed using SuperScript ® II-RNase$^-$
282 (Invitrogen) according to Invitrogen's protocol. The resulting cDNA products were amplified
283 with gene-specific primers. To obtain the full-length K_V2.1 and K_V2.2 clones from rabbit
284 urethra cDNAs, oligonucleotide primers were designed using Genetyx-Win software (Ver.
285 4.0, Genetyx Corp., Tokyo, Japan) as follows: K_V2.1 (+):5'-
286 CTCCGAATTCTCGAGTGACAGCGGCCT-3' corresponding to nucleotides 122-138 and (-
287):5'-CTCCTCTAGATCAGAGGAACAGCCCCCCCACT-3' corresponding to nucleotides
288 2824-2803 of rabbit K_V2.1 (GenBank accession number NM_001082087, CDS: 175-2751);
289 K_V2.2 (+):5'-CTCCAAGCTTAACTGTCATGCTTGCCCCG-3' corresponding to
290 nucleotides 98-116 and (-):5'-CTCCTCTAGACTAGTCACATGCTGGTCTCCCG-3'
291 corresponding to nucleotides 2923-2902 of rabbit K_V2.2 (NM_001082137, CDS: 184-2919).
292 The sequences underlined are *EcoR* I (GAATTC), *Hind* III (AAGCTT) and *Xba* I
293 (TCTAGA) recognition sites which were added to insert the PCR products into vector
294 plasmid DNA, pcDNA3.1(+)/Neo^r or pcDNA3.1(+)/Zeo^r (Invitrogen) in the proper
295 orientation. The thermal cycler program used for PCR amplification included a 0.5 min
296 denaturation step at 94 ^oC, a 0.5 min annealing step at 55 ^oC and a 3 min primer extension
297 step at 72 ^oC for 40 cycles. Reaction products were separated on 1 % agarose gels in Tris
298 acetate/EDTA buffer and were recovered from gel fragments using GENECLEAN II
299 (Qbiogene, Carlsbad, CA, USA). After restriction enzyme digestion, the amplified products

300 for $K_v2.1$ and $K_v2.2$ were ligated into *EcoR* I/*Xha* I and *Hind* III/*Xba* I recognition sites of
301 pcDNA3.1(+)/Neo^r and pcDNA3.1(+)/Zeo^r, respectively (pcDNA-rbK$_V$2.1, pcDNA-
302 rbK$_V$2.2). Sequence homology of cloned cDNAs was confirmed by DNA sequence analysis
303 with an ABI PRISM (model 310) (Applied Biosystems, Foster City, CA, USA). The HEK-
304 293 cell line was obtained from Health Science Research Resources Bank (HSRRB) (Tokyo,
305 Japan) and maintained in complete DMEM containing penicillin (100 units/ml) and
306 streptomycin (100 μg/ml). A mammalian expression vector was used for stable transfection
307 by calcium phosphate precipitation and then 1 mg/ml geneticine (Invitrogen) (for pcDNA-
308 rbK$_V$2.1) and zeocine (Invitrogen) (for pcDNA-rbK$_V$2.2)-resistance cells were selected and
309 identified by RT-PCR analysis, respectively.
310
311 **Immunocytochemistry**
312 Single cells were plated on 35 mm glass bottom culture dishes and culture medium was
313 removed from HEK cells prior to staining. Cells were washed in PBS and fixed in a solution
314 containing 2% paraformaldehyde (PFA, for $K_v2.1$ and $K_v2.2$ antibodies) made up in
315 phosphate buffered saline (PBS) or acetone (for $K_v9.3$ antibody) for 20-30 mins. The fixative
316 was then removed and cells were washed 3 times in PBS at 5 min intervals. Cells were
317 permeabilised in a PBS solution containing 0.3% Triton X and 3% goat serum for 10 mins.
318 Cells were again washed in 3 times with PBS at 5 min intervals.
319 Primary antibodies were prepared as per manufacturer's instructions and optimized for use
320 with this cell type. The primary antibodies (Alomone Laboratories, Israel) were incubated
321 with the cells overnight at 4°C in a humidified box. Primary antibody was removed and cells
322 were washed a further 3 times with PBS. The secondary antibody, Alexa 488 anti-rabbit
323 (Invitrogen, $K_v2.1$ & $K_v2.2$), or anti-goat (Invitrogen, $K_v9.3$) was prepared at a 1:1000
324 dilution in 1 ml PBS with 3% goat serum. Cells were incubated in secondary antibody at 4°C
325 for 1 hour. Cells were washed with PBS 5 times prior to imaging. Dishes were mounted
326 onto and imaged with an upright Axioskop 2 LSM 510 Meta confocal microscope (Zeiss).
327 Cells were excited with a 488 nm laser and emission was detected at >505 nm.
328
329 **Western Blotting**
330 Protein fractions of the plasma membrane were prepared from HEK293 cells according to the
331 Alomone Laboratory protocol (http://www.alomone.com). Protein fractions were solubilized
332 with sample buffer including 1% SDS and subjected to SDS-PAGE (10%). The blots were

333 incubated with anti-$K_V2.1$ or anti-$K_V2.2$ antibody (Alomone Labs, Jerusalem, Israel), and
334 then incubated with anti-rabbit horseradish peroxidase-conjugated IgG (Chemicon,
335 Temecula, CA, USA). An enhanced chemiluminescence detection system (Amersham
336 Biosciences, Piscataway, NJ, USA) was used for the detection of the bound antibody.
337 Resulting images were analyzed by a LAS-1000 device (Fujifilm, Tokyo, Japan). Primary
338 antibody preincubated with excess antigen was tested for specificity confirmation.
339
340 **Tension Recordings**
341 Strips of smooth muscle (8 x 1 x 1 mm) were removed from the rabbit urethra, placed in
342 water-jacketed organ baths maintained at 36±1°C, and perfused with warmed Krebs solution
343 that was bubbled with 95% O_2-5% CO_2 and contained atropine (1 μM), guanethidine (1 μM)
344 and N^G-Nitro-L-arginine (NO-ARG, 100 μM) to block any contribution from
345 neurotransmitters. Strips were adjusted to a tension of 2–4 mN and allowed to equilibrate for
346 50 min before experimentation began. Contractions were measured using the multi channel
347 Myobath system and data was acquired using DataTrax 2 software (WPI, Europe).
348
349 **Drugs used:**
350 Amphotericin B, atropine, guanethidine, N^G-Nitro-L-arginine, α-dendroxin, κ-dendrotoxin
351 and Pen A were all obtained from Sigma. Stromatoxin and margatoxin were supplied by
352 Alomone Labs, Israel. Iberiotoxin was obtained from Tocris. All drugs were made up in the
353 appropriate stock solution before being diluted to their final concentrations in Hank's
354 solution.
355
356 **RESULTS**
357 Using our dispersal procedure, relaxed urethral smooth muscle cells (RUSMC) and
358 interstitial cells (ICC) could be reliably isolated from the rabbit urethra. The SMC were
359 easily distinguished from the ICC as they were unbranched, spindle shaped, and contractile.
360
361 **Blockade of BK current unmasks a K_v current in RUSMC.**
362 In this set of experiments, currents were recorded using the perforated patch configuration of
363 the patch clamp technique. Under voltage clamp at –60 mV, the SMC were electrically
364 quiescent as demonstrated previously (33). When cells were depolarized from –60 mV to +40
365 mV for 500 ms, large transient and sustained outward currents were evoked (Figures 1A and

366 1C). We first examined the effects of the selective large conductance Ca^{2+} activated K^+ (BK)
367 channel toxin, iberiotoxin (IbTx, 300 nM) on these currents in order to ascertain if they were
368 due to activation of BK channels. As Figure 1A suggests, application of IbTx abolished the
369 transient current and also reduced the amplitude of the sustained current. A summary
370 barchart for 3 similar experiments is shown in Figure 1B. Under control conditions, the peak
371 current was 1767 ± 307 pA at +40 mV and this was significantly reduced in IbTx to 622 ±
372 142 pA ($p<0.01$, paired t-test). We also examined the effects of the BK channel blocker Pen
373 A, 100 nM) on the outward current evoked by a step to +40 mV and as Figure 1C suggests,
374 blockade of the BK current unmasked a slowly activating, sustained outward current. Figure
375 1D shows summary data obtained from 5 cells in which Pen A significantly reduced the peak
376 outward current at +40 mV from 1456 ± 258 pA to 438 ± 179 pA ($p<0.05$). Taken together,
377 these data suggest that the transient current and a component of the sustained current in
378 urethral SMC is due to the activation of BK channels and when this is blocked, a slowly
379 activating K_v current is unmasked. In a separate set of experiments the effects of IbTx were
380 assessed after Pen A application and it was found to have no additional effect (n=5).
381 Similarly, application of Pen A (100 nM) after application of IbTx (300 nM) failed to further
382 reduce the currents (n=3), suggesting that Pen A selectively blocks BK current in these cells.
383 To study the K_v current in more detail, all subsequent voltage clamp experiments on RUSMC
384 were carried out in the presence of 100 nM Pen A.
385 The upper panel of Figure 1E shows the voltage protocol used to evoke K_v currents in
386 RUSMC, which involved holding the cell at –60 mV and depolarizing it from –80 mV to +50
387 mV in 10 mV steps for 500 ms before repolarising back to –40 mV. These experiments were
388 carried out in Ca^{2+} free Hanks solution to remove contaminant Ca^{2+} currents (6, 18). As the
389 lower panel of Figure 1E suggests, outwardly rectifying, sustained currents were recorded in
390 response to these depolarizing voltage steps and large, slowly-deactivating, tail currents were
391 evoked upon repolarisation to –40 mV. Figure 1F shows a summary current voltage (IV) plot
392 taken from 18 cells and illustrates that the K_v current was activated at potentials positive to –
393 50 mV.
394
395 **Evidence that K_v1 channels do not contribute to the K_v current in rabbit urethral**
396 **myocytes.**
397 Given that K_v1 channels have been shown to play an important role in smooth muscle
398 excitability (1, 3, 4, 8, 16, 32, 38), we first determined if these channels contributed to this

399 current by examining the effects of a variety of K_v1-specific toxins on currents evoked by
400 steps from –60 to +40 mV. As Figure 2A illustrates, application of the $K_v1.1$/ $K_v1.2$/ $K_v1.6$
401 blocker α-dendrotoxin (100 nM, gray trace) did not inhibit the current, even though it has
402 been shown to block K_v1 channels in the nanomolar range (15, 29). In three similar
403 experiments, application of α-dendrotoxin failed to significantly alter the current (control
404 was 575 ± 53 pA compared with 617 ± 45 pA in α-dendrotoxin). Similarly, the $K_v1.1$ blocker
405 κ-dendrotoxin did not block the current (Figures 2C & 2D, 515 ± 61 pA in control compared
406 to 498 ± 57 pA in toxin, n=5). Application of the pan-K_v1 blocker margatoxin (100nM) was
407 also without effect as shown in Figure 2E. In three experiments, application of this toxin had
408 no significant effect on the K_v current (control was 686 ± 99 pA compared to 669 ± 102 pA,
409 n.s.). Taken together, these data suggest that the K_v current in rabbit urethral myocytes is
410 unlikely to be due to homomers or heteromers of K_v1 subunits.
411
412 **Evidence that K_v2 channels do contribute to the K_v current in rabbit urethral myocytes.**
413 To test if K_v2 channels were functionally expressed in rabbit urethral smooth muscle cells,
414 we examined the effects of the K_v2 channel gating modifier, ScTx on families of currents
415 evoked by steps from –80 to +50mV in 10 mV increments from a holding potential of –100
416 mV. When cells were stepped back to –60 mV, outward tail currents were difficult to resolve.
417 Escoubas *et al.,* (2002) have previously shown that 100 nM ScTx reduced the amplitude of
418 $K_v2.1$ currents in COS cells evoked by a step to +50 mV by ~75%. As Figures 3B & 3C
419 demonstrate, application of 100 nM ScTx reduced the amplitude of the RUSMC currents.
420 Figure 3D shows summary IV plots of the K_v currents in the absence (open circles) and
421 presence (filled circles) of ScTx obtained from 12 cells. ScTx significantly reduced the
422 amplitude of currents at potentials positive to –30 mV and the toxin appeared to block more
423 effectively at negative membrane potentials. Thus, at 0 mV the peak current was reduced by
424 ~70% from 306 ± 67 pA to 94 ± 20 pA compared to only 50% blockade at +50 mV, where
425 the currents were reduced from 961 ± 182 pA to 460 ± 93 pA in the presence of ScTx.
426 We next used RT-PCR to examine the expression profile of message for the K_v2 family
427 members. As Figure 4A demonstrates, PCR products for $K_v2.1$ (upper panel, expected
428 amplicon=196 bp) and $K_v2.2$ (lower panel, expected amplicon=146 bp) were amplified from
429 brain tissue (Br) and strips of urethra taken from 4 animals (Ur_1-Ur_4), but were absent in the
430 non-template controls (NTC). To examine the quantitative expression of the two K_v2

431 subtypes in urethra (relative to β-actin), we performed qPCR on urethral strips taken from 6
432 animals. As Figure 4B suggests, there was robust expression of $K_v2.1$ and $K_v2.2$ mRNA, but
433 there was no significant difference in transcriptional expression levels between the two
434 subtypes (paired t-test). When we examined the transcriptional expression of $K_v1.2$, $K_v1.3$,
435 $K_v1.7$, $K_v4.2$ and $K_v4.3$ in three strips, we found that they were approximately 3-fold lower
436 than either of the K_v2 family members.
437 Given that the transcriptional expression data were obtained from tissue strips, rather than
438 isolated cells, it is possible that the data reflect K_v2 transcriptional expression in nerves or
439 blood vessels in the urethra. Therefore, to test if K_v2 was expressed in isolated RUSMC, we
440 next performed immunocytochemistry with specific anti-$K_v2.1$ and anti-$K_v2.2$ antibodies. As
441 Figure 4C shows, membrane limited staining was obtained only when primary and secondary
442 antibodies (Figure 4Cii) raised against $K_v2.1$ were present. No immunoreactivity to $K_v2.1$
443 was detected when the antibody was incubated with an excess of antigen (data not shown).
444 When cells were incubated with monoclonal mouse anti-$K_v2.2$ primary antibodies
445 (Antibodies Inc., Davis, USA) and stained with a goat anti-mouse Alexa 488 secondary
446 antibody, some immunoreactivity was observed (Figure 4Dii). Patchy staining appeared to
447 be largely confined to membrane-bound areas although some intracellular staining was also
448 present throughout the cells. It is unclear if this was a result of poor antibody interaction or
449 reflective of actual $K_v2.2$ distribution. However, secondary controls in which the primary
450 antibody was omitted showed no immunoreactivity (Figure 4 Div).
451
452 **Comparison of the native ScTx sensitive current with Kv2.1 and Kv2.2 channels cloned**
453 **from the rabbit urethra.**
454 Having established that the majority of the K_v current in RUSMC was ScTx sensitive, we
455 next cloned $K_v2.1$ and $K_v2.2$ from the rabbit urethra and stably expressed them in HEK 293
456 cells. We performed immunocytochemistry with specific anti-$K_v2.1$ and anti-$K_v2.2$
457 antibodies detailed above on each clone of the K_v2 channel. As Figure 5A shows, membrane
458 limited staining of $HEK_{Kv2.1}$ cells was obtained only when primary and secondary antibodies
459 (Figure 5Aii) raised against $K_v2.1$ were present. No immunoreactivity to $K_v2.1$ was detected
460 when the antibody was incubated with an excess of antigen (data not shown). Similarly, the
461 $HEK_{Kv2.2}$ were only immunopositive when incubated with both primary and secondary
462 antibodies (Figure 5Bii).

463 We confirmed the molecular weights of $K_V2.1$ and $K_V2.2$ proteins cloned from rabbit urethra
464 in HEK cells by Western blotting. Figures 5C & 5D show bands around 100 and 110 kDa
465 were detected, consistent with the molecular weights predicted from rabbit $K_V2.1$ (95 kDa)
466 and $K_V2.2$ (102 kDa), respectively in the stably-transfected cells (middle lanes), but not the
467 vector-transfected HEK cells (left lanes). This immunoreactivity was decreased following
468 preincubation of anti-$K_V2.1$ and anti-$K_V2.2$ antibodies with excess antigens, respectively
469 (right lanes).
470 To compare the biophysical and pharmacological properties of the native K_v current with
471 currents in $HEK_{Kv2.1}$ and $HEK_{Kv2.2}$ cells we used the ruptured patch configuration of the
472 patch clamp technique. As a control, current voltage (IV) relationships were determined from
473 non-transfected HEK cells to measure the amplitude of endogenous currents. In three cells
474 the mean amplitude of currents evoked by a depolarizing step to +60 mV was +380 ± 126
475 pA, suggesting that the endogenous currents were unlikely to contaminate our recordings
476 significantly.
477 Figure 6 shows that $HEK_{Kv2.1}$, $HEK_{Kv2.2}$ and RUSMC K_v currents had similar kinetics and
478 voltage dependent activation. However a much slower tail current was observed in the native
479 RUSMC (Figure 6A) in response to a repolarising step to –40 mV, compared to the $HEK_{Kv2.1}$
480 and $HEK_{Kv2.2}$ cells. Figures 6A and 6B show typical currents and summary activation curves
481 respectively, of the ScTx-sensitive (100 nM) difference currents obtained in freshly dispersed
482 RUSMC in which the mean activation $V_{1/2}$ was –7 ± 5 mV (n=12). This was not significantly
483 different to the activation $V_{1/2}$ obtained from $HEK_{Kv2.1}$ (0 ± 5 mV, n=10, Figure 6D) or
484 $HEK_{Kv2.2}$ cells (0±1 mV, n=8, Figure 6F).
485 To examine the kinetics of the currents in more detail, we first measured the activation time
486 constants of the RUSMC ScTx-sensitive currents and compared these with the $HEK_{Kv2.1}$ and
487 $HEK_{Kv2.2}$ currents. As Figure 7A suggests, the activation time constants of all three currents
488 decreased with depolarization. The $HEK_{Kv2.1}$ currents (filled circles, n=10) had slower
489 activation time constants than $HEK_{Kv2.2}$ (filled squares, n=10) at potentials negative to 0 mV.
490 However at positive potentials, the activation time constants of the currents in $HEK_{Kv2.1}$ and
491 $HEK_{Kv2.2}$ cells were indistinguishable from each other, and both were significantly different
492 to the RUSMC ($p<0.05$, ANOVA). Similarly, as shown in Figure 7B, the deactivation time
493 constants in $HEK_{Kv2.1}$ (26 ± 14 ms, n=10, range 6-122 ms), and $HEK_{Kv2.2}$ cells (9 ± 1 ms,
494 n=10, range 7-14 ms) were not significantly different, although there was more variation in
495 the $HEK_{Kv2.1}$ currents. A much more slowly deactivating tail current was evident in the

496 RUSMC (Figure 7B, τ=322 ± 91 ms, n=14, $p<0.05$, ANOVA). There was considerable
497 variation in the rate of deactivation of the RUSMC K_v current and the time constant in these
498 cells ranged from 66 ms to 1300 ms. These data suggest that there may be some
499 heterogeneity in the ion channel expression perhaps caused by the variable expression of
500 silent K_v subunits.
501 To assess if the slow tail current deactivation in RUSMC was due to the presence of silent K_v
502 subunits in RUSMC, we next compared the quantitative transcriptional expression of a
503 number of silent family members. As Figure 7C suggests transcriptional expression of K_v9.3
504 was highest of all the members tested. To check if the isolated RUSMC showed functional
505 expression of this modulatory subunit, we used immunocytochemistry with specific anti-
506 K_v9.3 antibodies. As Figure 7D shows, membrane limited staining was obtained only when
507 primary and secondary antibodies (Figure 7Dii) raised against K_v9.3 were present, suggesting
508 that this regulatory K_v subunit was present in RUSMC.
509
510 We next examined the voltage dependence of steady state inactivation of the three currents
511 using a standard double pulse protocol. Cells were subjected to 10s conditioning steps from –
512 100 mV to 0 mV in 10 mV increments before stepping to a test potential of +40 mV for 500
513 ms to maximally activate the K_v current. Figures 8A, C and E shows typical recordings of the
514 currents obtained by the step to +40 mV following the preceding conditioning potentials in
515 RUSMC, $HEK_{Kv2.1}$ and $HEK_{Kv2.2}$ cells respectively. When these data were normalized,
516 plotted and fitted with the Boltzmann equation, inactivation $V_{1/2}$'s of –56±3 mV, -55±3 mV
517 and –30±3 mV were obtained for the native RUSMC (Figure 8B, n=9), K_v2.1 (Figure 8D,
518 n=13) and K_v2.2 (Figure 8F, n=11) currents respectively. There was no significant difference
519 in the inactivation $V_{1/2}$ between the native RUSMC current and the $HEK_{Kv2.1}$ current, but
520 both were significantly different to the $HEK_{Kv2.2}$ current ($p<0.05$, ANOVA). These data
521 suggest that the steady state inactivation properties of the native RUSMC K_v currents are
522 more similar to $HEK_{Kv2.1}$ than $HEK_{Kv2.2}$ currents.
523
524 To establish the sensitivity of the currents to ScTx, we examined the effects of increasing
525 concentrations on currents evoked by a step to +40 mV. Figures 9A, C & E show typical
526 currents obtained in the absence and presence of increasing concentrations of ScTx in
527 RUSMC, $HEK_{Kv2.1}$ and $HEK_{Kv2.2}$ cells respectively. Unfortunately, we did not use
528 sufficiently high concentrations of ScTx to permit the construction of full concentration

529 effect curves, but the data show that ScTx caused a concentration dependent reduction of the
530 currents. When the summary data were plotted for RUSMC (Figure 9B), $HEK_{Kv2.1}$ (Figure
531 9D) and $HEK_{Kv2.2}$ currents (Figure 9F), we estimated the IC_{50} to be ~130 nM, ~150 nM and
532 ~70 nM respectively.
533
534 **Contribution of the ScTx sensitive current to evoked action potentials in rabbit urethral**
535 **myocytes.**
536 Having established that the majority of the K_v current in RUSMC was ScTx sensitive and
537 likely to be due to K_v2.1 subunits, we next assessed its contribution to electrical activity by
538 examining the effects of ScTx on evoked action potentials (AP). In these experiments the
539 perforated patch configuration of the patch clamp technique was used and a small
540 hyperpolarizing current was continually injected to bring the membrane potential to ~-60
541 mV. Figure 10A shows the results of a typical current clamp experiment in which an AP was
542 evoked by injecting 100 pA current for 40 ms into a RUSMC. This elicited an AP that
543 consisted of a rapid upstroke, a rapid repolarisation and an after-hyperpolarisation. When
544 ScTx (300 nM) was applied and the AP was evoked (green trace, Fig 10A) neither the
545 amplitude or duration of the AP or after-hyperpolarisation were significantly altered.
546 One explanation for this lack of effect, could be due to differences in the amplitude and
547 activation kinetics of the BK and K_v current. For example, a depolarising step to 0 mV
548 evokes a transient BK current of ~ 800 pA in amplitude in RUSMC and this current reaches
549 peak amplitude in less than 20 ms. In contrast, depolarisation evokes a K_v current in these
550 cells that is ~ 250 pA in amplitude at 0 mV (Figure 1F) and takes approximately 100 ms to
551 fully activate. Thus, at the peak of the AP, the K_v current would only reach ~ 25% of its peak
552 amplitude, due to the slow time course of its activation. We might therefore expect that the
553 contribution of the K_v current is only observed when the BK current is absent. To test this
554 directly, we first blocked the BK current with Pen A and then observed the effects of ScTx
555 application on the AP. Figure 10B shows a typical example of such an experiment where
556 Pen A (100 nM, Figure 10B, red line) increased the amplitude and duration of the AP.
557 Subsequent application of ScTx (300nM, green line) further prolonged the AP. Figure 10C
558 shows summary data from 5 cells in which the duration of the AP was recorded under control
559 conditions (open bars), in the presence of Pen A (100 nM, red bar) and in the presence of Pen
560 A and ScTx (300 nM, green bar). Pen A significantly increased the mean duration of the AP
561 from 24 ± 3 ms to 104 ± 17 ms ($p<0.05$) and this was further increased to 220 ± 61 ms

562 ($p<0.01$) following ScTx application. Although ScTx prolonged the AP, it had very little
563 effect on its peak amplitude (Figure 10D).
564
565 **Contribution of the ScTx sensitive current to contractile activity in strips of rabbit**
566 **urethra.**
567 To examine the contribution of K_v2 currents to spontaneous mechanical activity, we recorded
568 isometric tension from strips of urethra smooth muscle and examined the effects of ScTx
569 (100 nM). All experiments were carried out in the presence of atropine (1 μM), guanethidine
570 (1 μM) and NO-ARG (100 μM) to block any contribution from neurotransmitters. In
571 seventeen strips taken from 8 animals, small spontaneous contractions (mean amplitude 0.48
572 ± 0.18 mN, range 0.1- 2.8 mN) occurred at a mean frequency of 4.4 ± 1.1 min^{-1} (range 0 -
573 14.2 min^{-1}). Figure 11A shows an example of spontaneous mechanical activity in the absence
574 (upper panel) and presence of 100 nM ScTx (lower panel), where there was a small increase
575 in the amplitude and frequency of contractions following ScTx application for 30 minutes.
576 Figures 11B and C show summary data for 7 similar experiments in which the mean
577 contraction amplitude and frequency respectively, were measured in the absence (open bars)
578 and presence (closed bars) of ScTx (100 nM) for up to 30 minutes. Neither contraction
579 amplitude nor frequency, were significantly altered in the presence of ScTx ($p>0.05$, paired t-
580 test).
581 We next compared the effect of ScTx on contractility in the presence of Pen A (100 nM,
582 Figure 11D). Application of Pen A by itself increased the amplitude of contraction from 0.42
583 ± 0.3mN to 0.93 ± 0.2 mN and contraction frequency from 3 ± 1.2 to 6.7 ± 1.3 min^{-1} ($n=10$,
584 $p<0.05$, ANOVA).
585 Subsequent application of ScTx in the continued presence of Pen A (Figure 11D, lower
586 panel) significantly increased contraction amplitude and frequency, demonstrating that
587 blockade of K_v2 channels under these conditions, dramatically affects urethral contractility.
588 Summary data for ten experiments shown in Figure 11E & F demonstrated that application of
589 Pen A and ScTx significantly enhanced contraction amplitude to 3.2 ± 0.7 mN and frequency
590 to 10.1 ± 1.4 min^{-1} (black bars, $p<0.05$, ANOVA).
591

592 **DISCUSSION**

593 The aim of this study was to characterise the K_v current in rabbit urethral smooth muscle
594 cells, examine its molecular identity and assess its contribution to the action potential and
595 spontaneous contractile activity. We found that approximately 30% of the net outward
596 current at 40 mV was carried via an IbTx and Pen A-insensitive current that activated and
597 inactivated slowly at physiological potentials. Our results suggest that the K_v current shares a
598 number of features with K_v2.1 channels cloned from this tissue and demonstrate that its
599 blockade can significantly prolong the action potential, but only when the transient BK
600 current is blocked.

601 Although K_v1 channels have been shown to play an important role in a variety of smooth
602 muscles (1, 3, 4, 8, 14, 16, 38), it appears unlikely that they contribute significantly to the K_v
603 current in RUSMC, since they were unaffected by a variety of K_v1 specific toxins. The
604 current was insensitive to margatoxin, κ- and α-dendrotoxin which have been shown
605 previously to block K_v1 family members (15, 16, 29) at much lower concentrations than
606 those used in this study.

607 The data presented here suggest that K_v2 channels are likely to contribute significantly to the
608 K_v current in urethral smooth muscle. Thus, transcriptional expression for both K_v2.1 and
609 K_v2.2 was detected in whole urethral strips and immunocytochemical data suggests that both
610 K_v2.1 and K_v2.2 channels are located in the membranes of freshly dispersed RUSMC.
611 Furthermore, the native K_v current in the present study was reduced in a concentration
612 dependent manner by the K_v2 gating modifier ScTx (2, 10, 41) with an IC_{50} of ~130 nM,
613 consistent with the idea that K_v2 subunits underlie the K_v current in these cells. However, it is
614 important to note that ScTx can also block some K_v4 family members (10), but we feel that
615 these effects were unlikely to account for our results given that the K_v current in RUSMC did
616 not share any of the biophysical properties of the 'A' type currents encoded by K_v4 family
617 members (12). It is possible that other K_v channel subtypes may also contribute to the
618 delayed rectifier current in RUSMC, but we have not examined this in the present study since
619 ~70% of the K_v current was abolished at physiological potentials by ScTx.
620

621 When we examined the biophysical properties of the K_v current in RUSMC, we found that
622 the currents activated with a $V_{1/2}$ of –7 mV, which is similar to those obtained in native cells

623 and heterologous expression systems expressing either $K_v2.1$ channels (4, 20, 21, 22, 25, 37,
624 39, 41) or $K_v2.2$ channels (19). Interestingly, the inactivation $V_{1/2}$ for the K_v current in
625 RUSMC was -56±3 mV and although this value is similar to that shown for $K_v2.1$ in native
626 pyramidal neurons (-62 mV, (11)) and bladder SMCs (-61 mV, (37)), it is 25 to 35 mV more
627 negative than that recorded from K_v2 channels in various expression systems (20, 22, 25, 27,
628 30). The observed differences in the $V_{1/2}$ of inactivation of K_v2 channels recorded in native
629 cells and heterologous expression systems have been well documented and are thought to be
630 due to the presence of additional electrically silent K_v subunits in native cells (23, 26, 41) or
631 differences in the phosphorylation status of the channel (21, 22). The silent K_v subunits
632 comprise the K_v5, K_v6, K_v8 and K_v9 families, which cannot form functional ion channels
633 when expressed alone, but can modify the biophysical properties when co-expressed with the
634 other pore forming K_v subunits (26, 27, 30, 31, 39, 41, 42). Thus, co-expression of $K_v2.1$
635 with the silent subunit $K_v9.3$ has been shown to slow deactivation, shift the activation $V_{1/2}$ by
636 ~-20 mV and alter the inactivation $V_{1/2}$ by ~-15 mV (26, 41). Similarly, co-expression of
637 $K_v2.1$ with either $K_v5.1$ or $K_v6.1$ shifted the inactivation $V_{1/2}$ by –30 mV to –57 mV and –66
638 mV respectively (20, 23, 27, 31). The presence of these silent subunits accounts for the
639 negative inactivation $V_{1/2}$ of $K_v2.1$ observed in mouse urinary bladder smooth muscle cells
640 (37), pyramidal neurones (11) and cerebral arterial myocytes (41), and may also be
641 responsible for the negative inactivation $V_{1/2}$ observed in RUSMC. Indeed, when we
642 compared the transcriptional expression of the silent K_v subunits in RUSMC, we found that
643 $K_v9.3$ message was ~4 fold higher than that of the other silent subunits tested and isolated
644 RUSMC were immunopositive to anti-$K_v9.3$ antibodies.
645 It is important to note that although there was no significant difference in the time constant of
646 deactivation between the $HEK_{Kv2.1}$ and $HEK_{Kv2.2}$ cells currents, there was more variation in
647 the deactivation time constants recorded from the $HEK_{Kv2.1}$ cells. Whether this is caused by
648 an up-regulation in silent K_v subunit expression in some of these stably transfected cells has
649 not been determined, but is worthy of further investigation.
650 Another possibility for the difference in inactivation $V_{1/2}$ between the rabbit $K_v2.1$ and other
651 homologues may due to the phosphorylation state of the channel. A number of studies have
652 demonstrated that steady state inactivation of $K_v2.1$ channels is significantly shifted by up to
653 35 mV in the negative direction by dephosphorylation (21, 22). Indeed the very negative
654 inactivation $V_{1/2}$ obtained in the native cells and the $K_v2.1$ channels expressed in HEK cells
655 in the present study are consistent with the idea that RUSMC $K_v2.1$ channels are in a hypo-

656 phosphorylated state. Whether this is a feature of rabbit $K_v2.1$ channels or specific to rabbit
657 urethral smooth muscle cells is unknown. Given that the $K_v2.1$ protein identified with
658 Western blotting was close to the predicted size, supports the idea that urethral K_v2 channels,
659 when expressed in HEK cells at least, are unlikely to be highly phosphorylated.
660 It is also important to note that we detected transcript for $K_v2.2$ in urethral smooth muscle
661 and some membrane bound staining for $K_v2.2$ in isolated RUSMC. Therefore, we can not
662 exclude the possibility that these channels, as homomers or heteromers with $K_v2.1$, may also
663 contribute to the K_v current in RUSMC.
664
665 **Role of K_v2 current in the urethra.**

666 To assess the contribution of the K_v2 current to the electrical activity of the RUSMC, we
667 examined the effects of ScTx on resting membrane potential (RMP) and on APs evoked by
668 brief current injections, as shown in Figure 10. Given that little K_v current is activated at –60
669 mV (see Figure 3D), it was not surprising that blockade of K_v2 channels had little effect on
670 RMP and suggests that these channels contribute little to setting the RMP. We were initially
671 surprised to find that ScTx, even at a concentration of 300 nM (which should block the
672 current by more than 50%), had little effect on the AP. Although Figure 10A suggests that
673 the duration of the AP afterhyperpolarisation was decreased in the presence of ScTx, this
674 effect was not found to be statistically significant. However, when the activation kinetics of
675 the transient BK current and the $K_v2.1$ current are compared, it is apparent that the $K_v2.1$
676 current activates sufficiently slowly that it, in contrast to the transient BK current, is unlikely
677 to contribute to the brief AP. However, when the BK current was inhibited with Pen A,
678 application of ScTx further increased the duration the AP, suggesting that under these
679 conditions at least, the K_v2 current contributes to the repolarisation phase of the AP. The
680 prolongation of the AP after K_v2 blockade would presumably increase Ca^{2+} influx and
681 enhance spontaneous contractions of the urethra. Indeed, when we examined ScTx on
682 spontaneous contractions, we observed that it alone had little effect on the amplitude
683 spontaneous contractions. However, when the BK channels were first blocked with Pen A,
684 inhibition of K_v2 current increased the amplitude of the contractions approximately threefold.

685 In summary, the results of this study suggest that the K_v current in RUSMC cells is likely to
686 be carried through $K_v2.1$ channels and that inhibition of this current prolongs the AP and
687 enhances contractile activity of the urethra, but only when the transient BK current is

688 inhibited. We have previously shown that noradrenaline can broaden the evoked AP by
689 inhibiting the transient BK current (40). It is possible that part of this effect may also be
690 mediated through regulation of K_v2 channels in these cells and future studies will examine if
691 these currents are regulated by excitatory and inhibitory neurotransmitters in the urethra.

692

693

694

695

696

697

ACKNOWLEDGEMENTS.

The authors would like to acknowledge the National Institutes of Health (NIDDK Grant number R01 DK68565) for funding this study. B.K was in receipt of a Ph.D. studentship from the Council of Directors, Ireland. This work was also supported by a grant from Takeda Science Foundation (S.O.), Science Foundation Ireland and the Health Research Board.

706 **REFERENCES**

707

708 1. Albarwani S, Nemetz LT, Madden JA, Tobin AA, England SK, Pratt PF, and
709 Rusch NJ. Voltage-gated K^+ channels in rat small cerebral arteries: molecular identity
710 of the functional channels. *J Physiol* **551**: 751–763, 2003
711
712 2. Amberg GC, Santana LF. Kv2 channels oppose myogenic constriction of rat cerebral
713 arteries. *Am J Physiol Cell Physiol*; **291(2):**C348-56. 2006
714
715 3. Amberg GC, Baker SA, Koh SD, Hatton WJ, Murray KJ, Horowitz B & Sanders KM.
716 Characterisation of the A-type potassium current in mouse gastric antrum. *J Physiol* **544**:
717 417-428. 2002
718
719 4. Archer SL, Souil E, Dinh-Xuan AT, Schremmer B, Mercier J C, El Yaagoubi A, Nguyen-
720 Huu L, Reeve HL, and Hampl V. Molecular identification of the role of voltage-gated K+
721 channels, Kv1.5 and Kv2.1, in hypoxic pulmonary vasoconstriction and control of resting
722 membrane potential in rat pulmonary artery myocytes. *J Clin Invest.* **101(11):** 2319–2330.
723 1998.
724
725 5. Brading AF. Spontaneous activity of lower urinary tract smooth muscles: correlation
726 between ion channels and tissue function. *J Physiol.* **570** (Pt 1): 13-22. 2006
727
728 6. Bradley JE, Anderson UA, Woolsey SM, Thornbury KD, McHale NG, Hollywood MA.
729 Characterization of T-type calcium current and its contribution to electrical activity in rabbit
730 urethra. *American Journal of Physiology.* Cell Physiol. **286(5)**: C1078-88. 2004
731
732 7. Chen M, Kellett WF, Petkov GV. Voltage-gated K^+ channels sensitive to stromatoxin-1
733 regulate myogenic and neurogenic contractions of rat urinary bladder smooth muscle
734 *American Journal of Physiology* - Regu Physiol**. 299(1):** R177-R184. 2010.
735
736 8. Cole WC & Clement-Chomienne O. Properties, regulation and role of potassium
737 channels in smooth muscle. *In Advances in Organ Biology*, vol. **8**, ed. Barr L & Christ GJ,
738 pp. 247–317. JAI Press, Stamford, Connecticut, USA. 2000
739
740 9. Cotton, K.D, Hollywood, M.A., McHale, N.G. & Thornbury, K.D. Ca^{2+}-current and
741 Ca^{2+}-activated chloride current in isolated smooth muscle cells of the sheep urethra. *Journal*
742 *of Physiology.* **505.1**, 121-131, 1997.
743
744 10. Escoubas P, Diochot S, Celerier ML, Nakajima T & Lazdunski M. Novel tarantula toxins
745 for subtypes of voltage-dependent potassium channels in the K_v2 and K_v4 subfamilies. *Mol*
746 *Pharmacol* **62,** 48-57, 2002.
747
748 11. Guan D, Tkatch T, Surmeier DJ, Armstrong WE & Foehring RC. K_v2 subunits underlie
749 slowly inactivating potassium current in rat neocortical pyramidal neurons. *J Physiol*;
750 **581**:941–60, 2007.
751 12. Gutman GA, Chandy KG, Grissmer S, Lazdunski M, McKinnon D, Pardo LA, Robertson
752 GA, Rudy B, Sanguinetti MC, Stuhmer W & Wang X. International Union of Pharmacology.

753 LIII. Nomenclature and molecular relationships of voltage-gated potassium channels.
754 *Pharmacol Rev* **57**:473–508, 2005
755
756 13. Hamill O.P., Marty A., Neher E., Sakmann B. and Sigworth F.J. Improved patch-clamp
757 techniques for high-resolution current recording from cells and cell-free membrane patches.
758 *Pflügers Arch.* **391** (2): 85-100, 1981.
759
760 14. Hart PJ, Overturf KE, Russell SN, Carl A, Hume JR, Sanders KM & Horowitz B.
761 Cloning and expression of a $K_v1.2$ class delayed rectifier K^+ channel from canine colonic
762 smooth muscle. *Proc Natl Acad Sci U S A* **90**, 9659–9663, 1993.
763
764 15. Harvey AL (2001). Twenty years of dendrotoxins. *Toxicon* 39(1),15-26. Review.
765
766 16. Hatton WJ, Mason HS, Carl A, Doherty P, Latten MJ, Kenyon JL, Sanders KM, and
767 Horowitz B. Functional and molecular expression of a voltage-dependent K(+) channel
768 ($K_v1.1$) in interstitial cells of Cajal. *J Physiol* **533**: 315-327, 2001.
769
770 17. Hollywood MA, McCloskey KD, McHale NG & Thornbury KD. Characterization of
771 outward K^+ currents in isolated smooth muscle cells from sheep urethra. *Am J Physiol Cell*
772 *Physiol*. **279** (2): C420-8, 2000.
773
774 18. Hollywood MA, Woolsey S, Walsh IK, Keane PF, McHale NG, Thornbury KD. T- and
775 L-type Ca^{2+} Currents in freshly dispersed smooth muscle cells from the human proximal
776 urethra. *J. Physiol.* **550**:753-64, 2003.
777
778 19. Johnston J, Griffin SJ, Baker C, Skrzypiec A, Chernova T & Forsythe ID. Initial segment
779 $K_v2.2$ channels mediate a slow delayed rectifier and maintain high frequency action potential
780 firing in medial nucleus of the trapezoid body neurons. *J Physiol*.; **586**: 3493–3509, 2008.
781
782 20. Kramer JW, Post MA, Brown AM & Kirsch GE. Modulation of potassium channel gating
783 by coexpression of $K_v2.1$ with regulatory $K_v5.1$ or $K_v6.1$ alpha-subunits. *Am J Physiol* **274**,
784 C1501–1510, 1998.
785
786 21. Misonou H, Mohapatra DP, Park EW, Leung V, Zhen D, Misonou K, Anderson AE &
787 Trimmer JS. Regulation of ion channel localization and phosphorylation by neuronal activity.
788 *Nat Neurosci* **7**: 711–718, 2004.
789
790 22. Mohapatra DP & Trimmer JS. The $K_v2.1$ C terminus can autonomously transfer $K_v2.1$-
791 like phosphorylation-dependent localization, voltage-dependent gating, and muscarinic
792 modulation to diverse Kv channels. *J Neurosci;* **26**: 685–95, 2006
793
794 23. Moreno-Domínguez A, Cidad P, Miguel-Velado E, López-López JR, Pérez-García MT.
795 (2009) De novo expression of $K_v6.3$ contributes to changes in vascular smooth muscle cell
796 excitability in a hypertensive mice strain. *J Physiol.* **587** (Pt 3):625-40. 2009
797
798 24. Ohya S, Tanaka M, Watanable M, Imaizumi Y. Diverse Expression of Delayed Rectifier
799 K^+ Channel Subtype Transcripts in Several Types of Smooth Muscles of the Rat. *Journal of*
800 *Smooth Muscle Research*, 36 (3). 101-115 (2000)
801

802 25. Ottschytsch N, Raes A, Van Hoorick D & Snyders DJ. Obligatory heterotetramerization
803 of three previously uncharacterized K_v channel alpha-subunits identified in the human
804 genome. *Proc Natl Acad Sci USA* **99**, 7986–7991, 2002.
805
806 26. Patel AJ, Lazdunski M & Honore E. $K_v2.1/K_v9.3$, a novel ATP-dependent delayed-
807 rectifier K^+ channel in oxygen-sensitive pulmonary artery myocytes. *EMBO J.* **16**, 6615–
808 6625, 1997.
809
810 27. Post MA, Kirsch GE & Brown AM. Kv2.1 and electrically silent $K_v6.1$ potassium
811 channel subunits combine and express a novel current. *FEBS Lett* **399**, 177–182, 1996.
812
813 28. Rae J., Cooper K., Gates P. & Watsky M. Low access resistance perforated patch
814 recordings using amphotericin B. *J. Neurosci. Methods.* **37**: 15-26, 1991.
815
816 29. Robertson B, Owen D, Stow J, Butler C, and Newland C. Novel effects of dendrotoxin
817 homologues on subtypes of mammalian K_v1 potassium channels expressed in Xenopus
818 oocytes. *FEBS Lett* 383: 26-30, 1996.
819
820 30. Salinas M, Duprat F, Heurteaux C, Hugnot JP & Lazdunski M. New modulatory a
821 subunits for mammalian Shab K^+ channels. *J Biol Chem* **272**, 24371–24379, 1997.
822
823 31. Sano Y, Mochizuki S, Miyake A, Kitada C, Inamura K, Yokoi H, Nozawa K,
824 Matsushime H & Furuichi K (2002). Molecular cloning and characterization of Kv6.3, a
825 novel modulatory subunit for voltage-gated K^+ channel Kv2.1. *FEBS Lett* **512**, 230–234
826
827 32. Schmalz F, Kinsella J, Koh SD, Vogalis F, Schneider A, Flynn ER, Kenyon JL &
828 Horowitz B. Molecular identification of a component of delayed rectifier current in
829 gastrointestinal smooth muscles. *Am J Physiol* **274**, G901–911, 1998.
830
831 33. Sergeant GP, Hollywood MA, McCloskey KD, Thornbury K.D. & McHale NG.
832 Specialised pacemaking cells in the rabbit urethra. *J Physiol.* **526** (2), 359-66, 2000.
833
834 34. Teramoto N, Brading A.F. Activation by levcromakalim and metabolic inhibition of
835 glibenclamide-sensitive K channels in smooth muscle cells of pig proximal urethra. *Br. J.*
836 *Pharmacol.* **118**:635–642, 1996.
837
838 35. Teramoto N, Brading A.F. The effects of nifedipine and other calcium antagonists on the
839 glibenclamide-sensitive K^+ currents in smooth muscle cells from pig urethra. *Br. J.*
840 *Pharmacol.* **123**:1601–1608, 1998.
841
842 36. Teramoto N, Creed, K.E., Brading A.F. Activity of glibenclamide-sensitive K^+ channels
843 under unstimulated conditions in smooth muscle cells of pig proximal urethra. *Naunyn-*
844 *Schmiedeberg's Arch. Pharmacol.*;**356**:418–424, 1997.
845
846 37. Thorneloe KS & Nelson MT. Properties and molecular basis of the mouse urinary bladder
847 voltage-gated K^+ current. *J Physiol* **549,** 65-74, 2003.
848
849 38. Tobin AA, Joseph BK, Albarwani S, Al-Kindi HN, Madden JA, Nemetz LT, Rusch NJ,
850 Rhee SW. Loss of cerebrovascular Shaker-type K^+ channels: a shared vasodilator defect of

851 genetic and renal hypertensive rats. Am J Physiol – Heart Circ Physiol, 297(1): H293-H303,
852 2009.
853
854 39. Vega-Saenz de Miera EC. (2004). Modification of K_v2.1 K+ currents by the silent K_v10
855 subunits. *Brain Res Mol Brain Res.* **123(1-2):**91-103. 2004.
856
857 40. Woolsey, S., Thornbury, KD., McHale, NG and Hollywood MA. Effects of
858 noradrenaline on transient BK current in freshly dispersed smooth muscle cells from the
859 rabbit urethra. *J Physiol* 543P S154, 2002
860 41. Zhong XZ, Abd-Elrahman KS, Liao CH, El-Yazbi AF, Walsh EJ, Walsh MP, Cole WC.
861 Stromatoxin-sensitive, heteromultimeric K_v2.1/K_v9.3 channels contribute to myogenic
862 control of cerebral arterial diameter. *J Physiol*. *J Physiol* **588,** 4519-4537. 2010.
863
864 42. Zhu XR, Netzer R, Bohlke K, Liu Q & Pongs O. Structural and functional
865 characterization of K_v6.2 a new g-subunit of voltage-gated potassium channel. *Receptors*
866 *Channels* **6**, 337–350, 1999.
867
868

869 **FIGURE LEGENDS**

870

871 **Figure 1. Blockade of transient BK current in USMC unmasks a slowly**
872 **activating outward current.** Currents were evoked from -60 mV to +40 mV for 500
873 ms and repolarised back to -60 mV. **A:** IbTx blocks BK current and unmasks a
874 delayed rectifier current. **B:** Approximately 30% of outward current is insensitive to
875 IbTx. **C:** Pen A also blocks the transient and sustained currents to unmask a K_v
876 current. **D:** Summary data showing the effect of Pen A on peak outward current
877 evoked by a step to +40 mV. **E:** Typical IV of the K_v currents. Note that large tail
878 currents were elicited when this cell was repolarised back to –40 mV. **F:** Summary
879 IV of K_v currents recorded in Ca^{2+} free and Pen A (n=18).

880

881 **Figure 2. RUSMC K_V current is resistant to K_v1 selective toxins.** Currents were
882 evoked in all experiments from -80 mV to +40 mV for 500 ms. **A:** Effect of α-
883 dendrotoxin on the K_v current from USMCs in the presence of Pen A. **B:** Summary
884 data from 3 cells in which α-dendrotoxin (filled bars) failed to inhibit the K_v current.
885 **C:** Effect of κ-dendrotoxin on the K_v current from USMCs in the presence of Pen A.
886 **D:** Summary data from 5 cells in which κ-dendrotoxin (filled bars) failed to inhibit the
887 K_v current. **E:** The pan-Kv1 blocker margatoxin (filled bars), also failed to block the
888 K_v current evoked by a step to +40 mV. **F**: Summary data from 3 cells.

889

890 **Figure 3. Rabbit USMC K_v current is sensitive to ScTx. A**: Typical family of
891 currents recorded in the absence of external Ca^{2+} and the presence of Pen A (100
892 nM). **B**: Currents from same cell in the presence of ScTx (100 nM). **C**: Summary IV
893 plots from 12 cells of peak outward current in the absence (open circles) and
894 presence (filled circles) of ScTx (100 nM).

895

896 **Figure 4. Transcriptional and immunocytochemical detection of K_v2 subtypes**
897 **in the rabbit urethra. A**: Upper panel shows transcriptional detection of $K_v2.1$
898 detected in control (brain) and strips of urethra (lower panel) from 4 animals.
899 Expected amplicon size=196 bp. Lower panel shows $K_v2.2$ detection in the same 5
900 tissues. Expected amplicon size= 149bp. No signal was detected in either non
901 template control (NTC). **B**: Q-PCR determination of $K_v2.1$ and $K_v2.2$ transcriptional

902 detection obtained from urethra from 6 animals. The expression of K_v2 message
903 (n=6, filled bars) was ~3 fold higher compared to $K_v1.2$, $K_v1.3$, $K_v1.7$, $K_v4.2$ or $K_v4.3$
904 (n=3, open bars). **C**: Transmitted light and fluorescent images obtained from freshly
905 dispersed RUSMC incubated with anti-$K_v2.1$ primary and secondary (Ci & Cii)
906 antibodies, or with secondary antibody alone (**Ciii** & **Civ**). **D**: Transmitted light and
907 fluorescent images obtained from freshly dispersed RUSMC incubated with anti-
908 $K_v2.2$ primary and secondary (**Di** & **Dii**) antibodies, or with secondary antibody alone
909 (**Diii** & **Div**). The calibration bars represent 20 μm.
910
911 **Figure 5. Immunocytochemical detection of K_v2 subtypes in HEK cells. A**:
912 Transmitted light and fluorescent images obtained from HEK cells stably transfected
913 with $K_v2.1$ and incubated with anti-$K_v2.1$ primary and secondary (**Ai** & **Aii**)
914 antibodies, or with secondary antibody alone (**Aiii** & **Aiv**). **B**: Transmitted light and
915 fluorescent images obtained from HEK cells stably transfected with $K_v2.2$ incubated
916 with anti-$K_v2.2$ primary and secondary (**Bi** & **Bii**) antibodies, or with secondary
917 antibody alone (**Biii** & **Biv**). The calibration bars represent 20 μm. **C:** Western blots
918 from membrane fractions obtained from vector transfected HEK cells (left lane), HEK
919 cells stably transfected with $K_v2.1$ (middle lane) and incubated with anti-$K_v2.1$
920 primary antibody in the presence of excess antigen (right lane) **D**. Western blots
921 from membrane fractions obtained from vector transfected HEK cells (left lane), HEK
922 cells stably transfected with $K_v2.2$ (middle lane) and incubated with anti-$K_v2.2$
923 primary antibody in the presence of excess antigen (right lane).
924
925 **Figure 6. Comparison of RUSMC ScTx-sensitive K_v current with currents from**
926 **HEK cells stably transfected with $K_v2.1$ and $K_v2.2$ channels. A**: A typical family of
927 ScTx difference currents obtained by digitally subtracting the current in the presence
928 of ScTx from the control currents. **B:** Mean activation data obtained from the ScTx-
929 sensitive difference currents from twelve RUSMC. Panels **C** and **D** show a typical
930 family of $K_v2.1$ currents and the associated activation curve, respectively. Panels **E**
931 and **F** show typical $K_v2.2$ currents and the summary activation curve, respectively.
932 The solid lines in Panels **B**, **D** & **F** show the Boltzmann fits of the mean data ± SEM.
933
934 **Figure 7. Evidence that RUSMC express silent K_v subunits. A:** Time constant of

935 activation is plotted against voltage for native cells (open circles) and HEK cells
936 expressing $K_v2.1$ (filled circles) and $K_v2.2$ (filled squares). **B:** Shows the deactivation
937 time constant measured following a repolarising step to -40 mV from 30 mV in native
938 cells (n=21) and HEK cells stably expressing $K_v2.1$ (n=10) and $K_v2.2$ (n=10). **C.** Q-
939 PCR data comparing the transcriptional expression of silent K_v subunits in the rabbit
940 urethra. **D.** Transmitted light and fluorescent images obtained from freshly dispersed
941 RUSMC and incubated with anti-$K_v9.3$ primary and secondary (Di & Dii) antibodies,
942 or with secondary antibody alone (Diii &Div).
943
944 **Figure 8. Steady-state inactivation of the native K_v current is similar to $K_v2.1$,**
945 **but not $K_v2.2$ channels stably expressed in HEK cells.** Standard double pulse
946 protocols shown in the inlay, were used to examine the steady-state voltage-
947 dependent inactivation of K_v currents in RUSMC (**A**), $K_v2.1$ (**C**) and $K_v2.2$ channels
948 (**E**) stably-expressed in HEK cells. Summary inactivation curves for native K_v in
949 RUSMC (**B**, n=9), $K_v2.1$ (**D**, n=13) and $K_v2.2$ channels (**F**, n=11) expressed in HEK
950 cells. The solid lines represent the Boltzmann fit to the data and the mean
951 inactivation $V_{1/2}$ is shown.
952
953 **Figure 9. Comparison of ScTx effect on native RUSMC K_v current compared to**
954 **$K_v2.1$ and $K_v2.2$ channels stably expressed in HEK cells.** ScTx produced a
955 concentration-dependent inhibition of native K_v currents (**A**), $K_v2.1$ (**B**), and $K_v2.2$ (**C**)
956 currents stably expressed in HEK cells. When summary data were normalised and
957 plotted against increasing concentrations of ScTx, there was little difference in the
958 estimated IC_{50} for ScTx on the native current (**B**, n=7), $K_v2.1$ (**D**, n=5) or $K_v2.2$ (**F**,
959 n=6) stably expressed in HEK cells.
960
961 **Figure 10. K_v2 blockade prolongs AP duration when BK channels are blocked.**
962 **A:** Current injection evoked a brief AP (black line) which was unaffected by ScTx
963 application (300 nM, green line). **B:** APs evoked in control (black line), Pen A (red
964 line) and ScTx plus Pen A (green line). **C:** Mean AP duration in control (white bar,
965 23.7 ± 3 ms), 100 nM Pen A (red bar, 104.8 ± 17 ms) and ScTx plus pen A (green
966 bar, 220.1 ± 61 ms, n=5). *D*: Average peak change in voltage for evoked AP in
967 control (white bar, 65.3 ± 5 mV), pen A (100 nM, red bar, 87.8 ± 1 mV) and pen A

968 plus ScTx (300 nM, green bar, 90.8 ± 3 mV, n=5).

969

970 **Figure 11. K_v2 blockade enhances contractions when BK channels are**
971 **blocked.**
972 **A:** Under control conditions, the urethra produced small amplitude contractions that
973 were little affected by application of ScTx (100 nM). Summary data from seven
974 experiments in which (**B**) contraction amplitude and (**C**) contraction frequency were
975 compared before (open bars) and during ScTx (filled bars). **D:** Application of Pen A
976 itself increased contraction frequency and amplitude and ScTx further enhanced this
977 effect. Summary data from seven experiments in which (**E**) contraction amplitude
978 and (**F**) contraction frequency were compared in the absence of any drugs (open
979 bars), after Pen A application (gray bars) and during Pen A and ScTx application
980 (black bars).

981
982
983
984
985
986
987
988
989

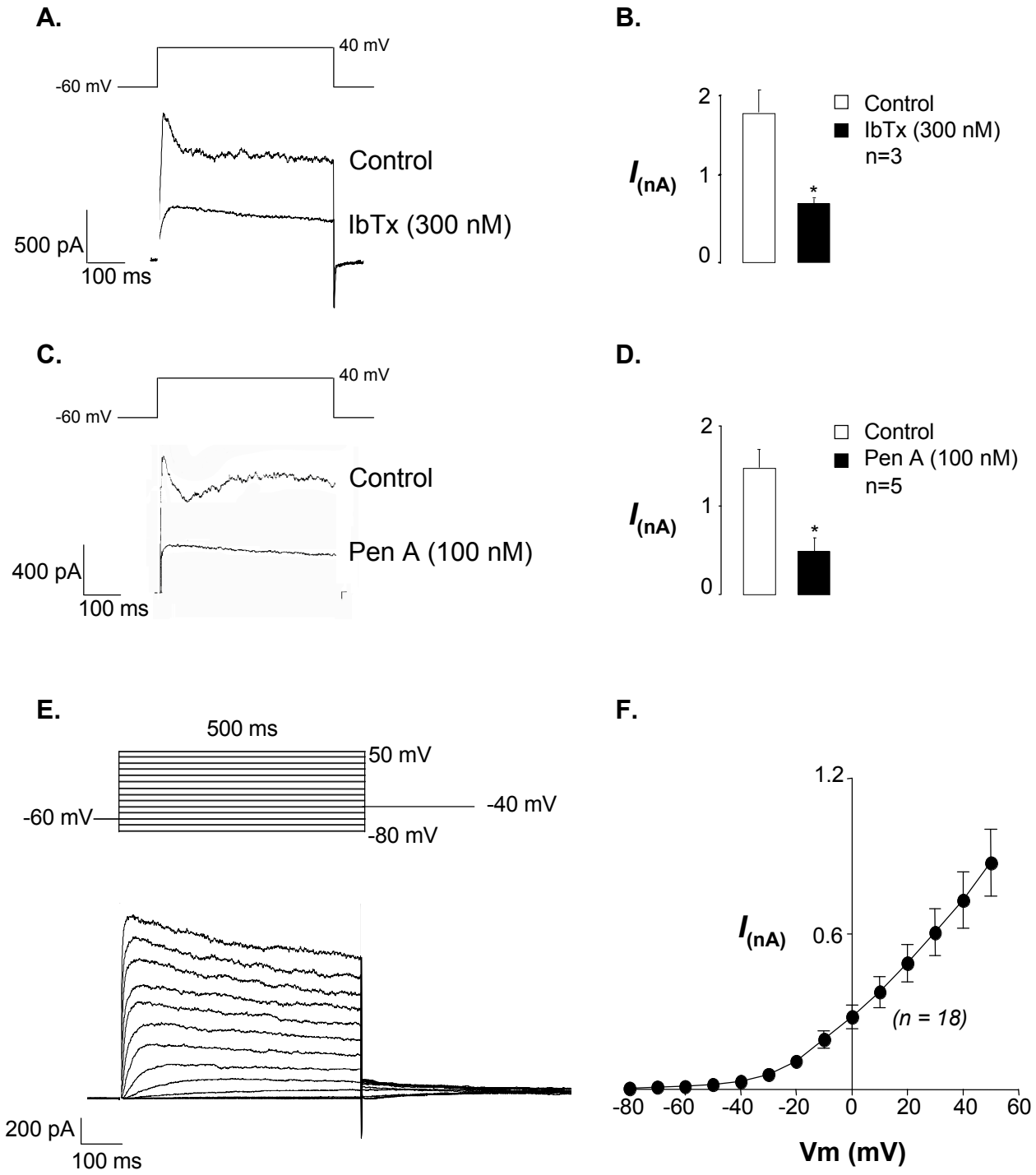
A.
40 mV
-60 mV
Control
IbTx (300 nM)
500 pA
100 ms
B.
2
1
0
I(nA)
Control
IbTx (300 nM)
n=3
*
C.
40 mV
-60 mV
Control
Pen A (100 nM)
400 pA
100 ms
D.
2
1
0
I(nA)
Control
Pen A (100 nM)
n=5
*
E.
500 ms
50 mV
-60 mV
-40 mV
-80 mV
200 pA
100 ms
F.
1.2
0.6
I(nA)
(n = 18)
-80 -60 -40 -20 0 20 40 60
Vm (mV)

Figure 1.

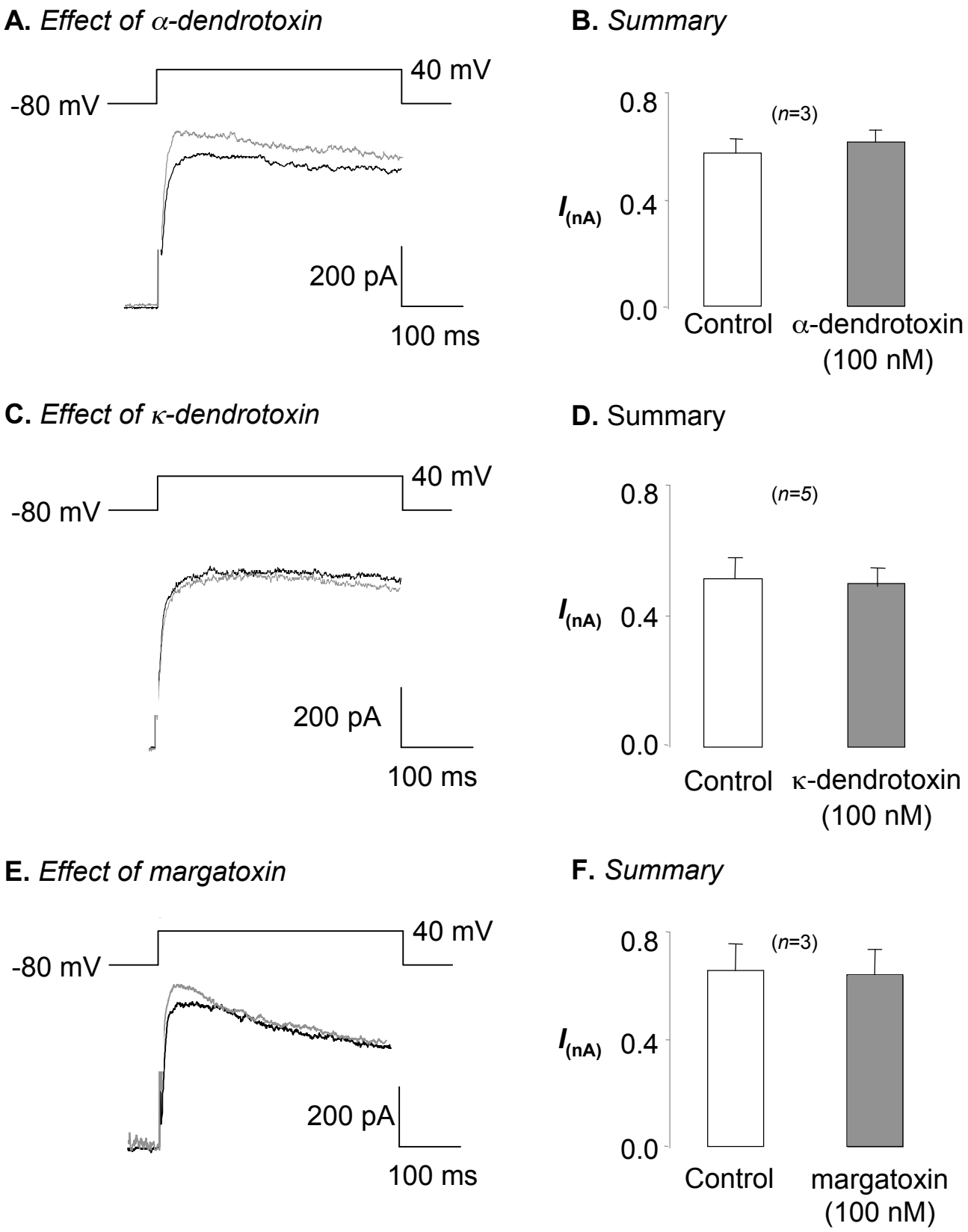
A. Effect of α-dendrotoxin
-80 mV
40 mV
200 pA
100 ms
B. Summary
0.8
0.4
0.0
I(nA)
(n=3)
Control
α-dendrotoxin
(100 nM)
C. Effect of κ-dendrotoxin
-80 mV
40 mV
200 pA
100 ms
D. Summary
0.8
0.4
0.0
I(nA)
(n=5)
Control
κ-dendrotoxin
(100 nM)
E. Effect of margatoxin
-80 mV
40 mV
200 pA
100 ms
F. Summary
0.8
0.4
0.0
I(nA)
(n=3)
Control
margatoxin
(100 nM)

Figure 2.

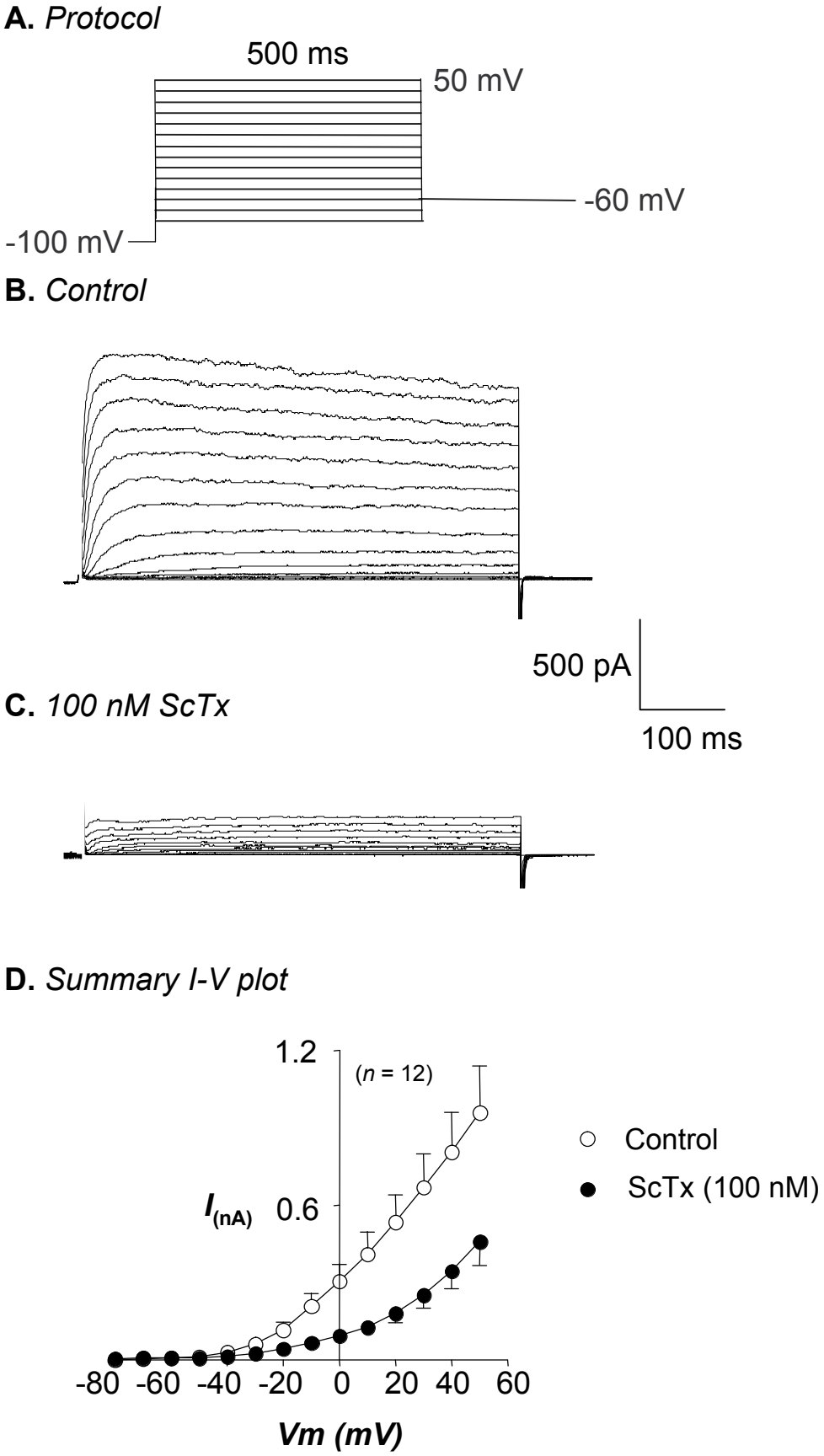
A. Protocol
500 ms
50 mV
-60 mV
-100 mV
B. Control
500 pA
100 ms
C. 100 nM ScTx
D. Summary I-V plot
1.2
(n = 12)
I(nA)
0.6
-80 -60 -40 -20 0 20 40 60
Vm (mV)
Control
ScTx (100 nM)

Figure 3.

A. *Detection of K_v2 transcripts*

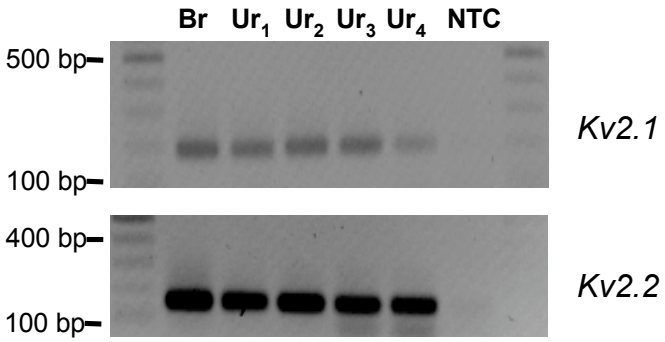

B. *Comparison of K_v transcription*

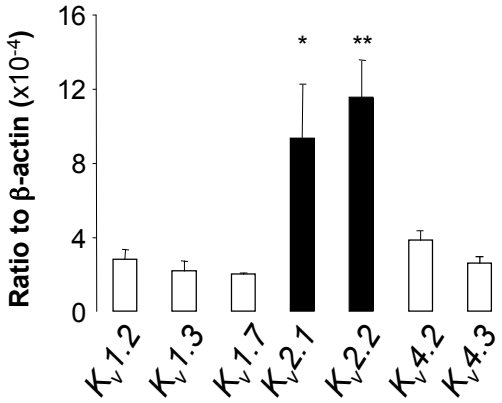

C. *K_v 2.1 immunoreactivity*

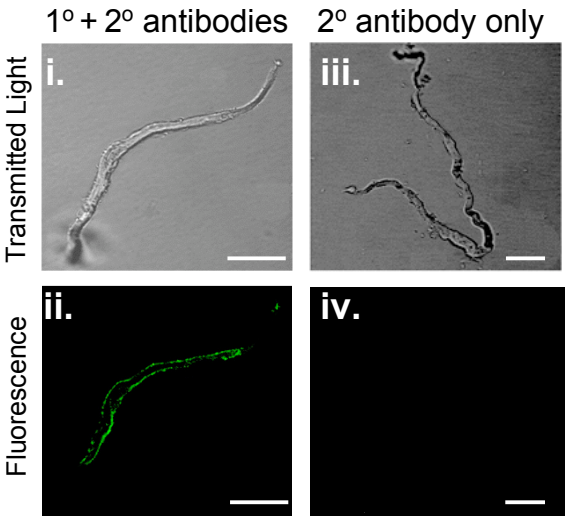

D. *K_v 2.2 immunoreactivity*

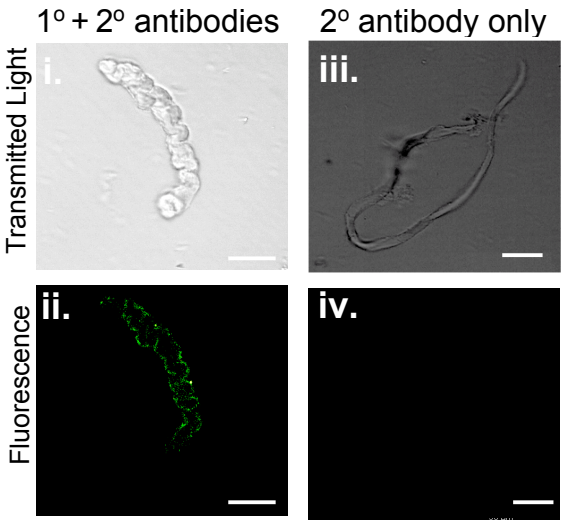

Figure 4.

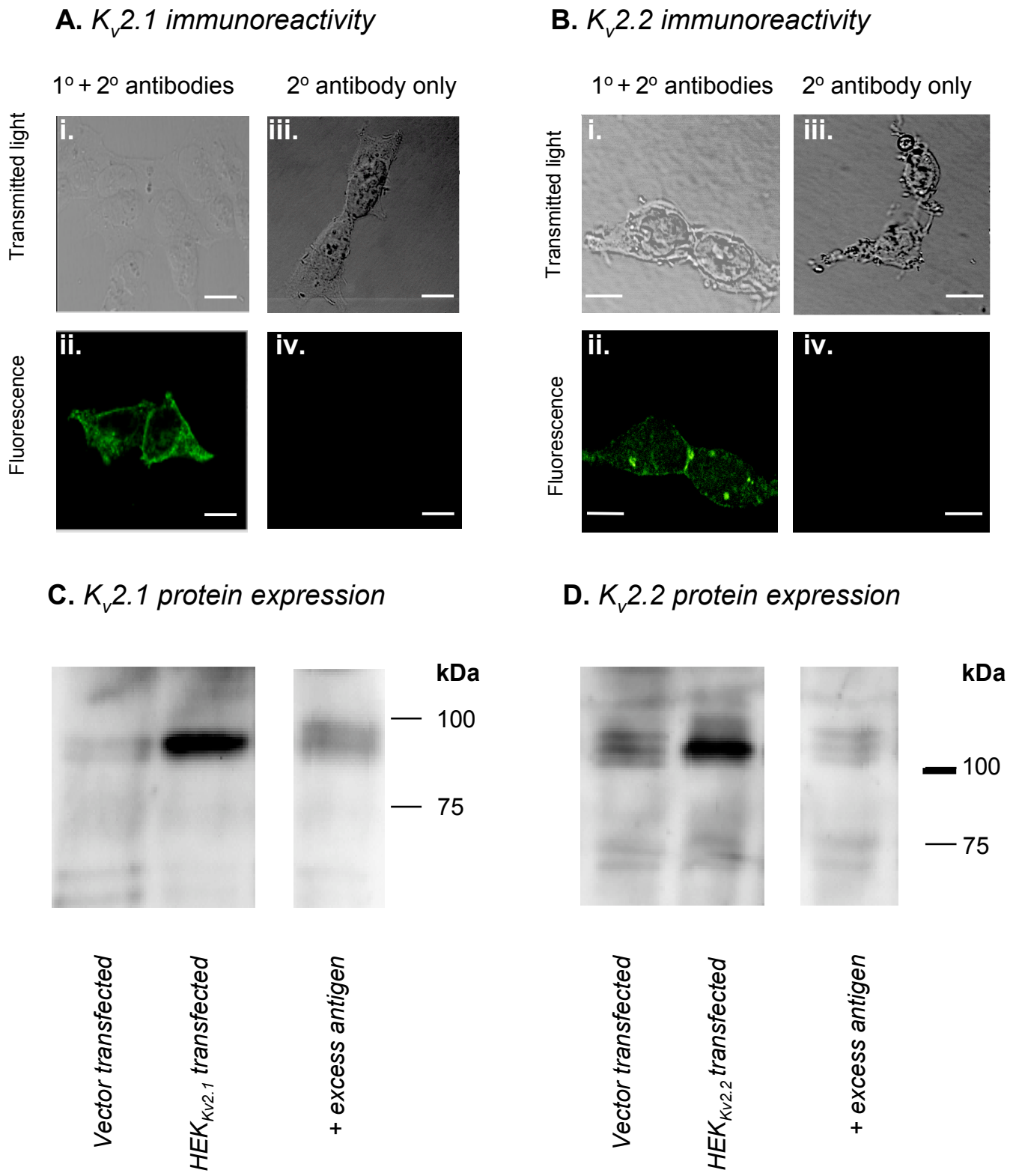
A. $K_v2.1$ immunoreactivity
1° + 2° antibodies
2° antibody only
Transmitted light
Fluorescence
i.
iii.
ii.
iv.
B. $K_v2.2$ immunoreactivity
1° + 2° antibodies
2° antibody only
Transmitted light
Fluorescence
i.
iii.
ii.
iv.
C. $K_v2.1$ protein expression
kDa
100
75
Vector transfected
$HEK_{Kv2.1}$ transfected
+ excess antigen
D. $K_v2.2$ protein expression
kDa
100
75
Vector transfected
$HEK_{Kv2.2}$ transfected
+ excess antigen

Figure 5.

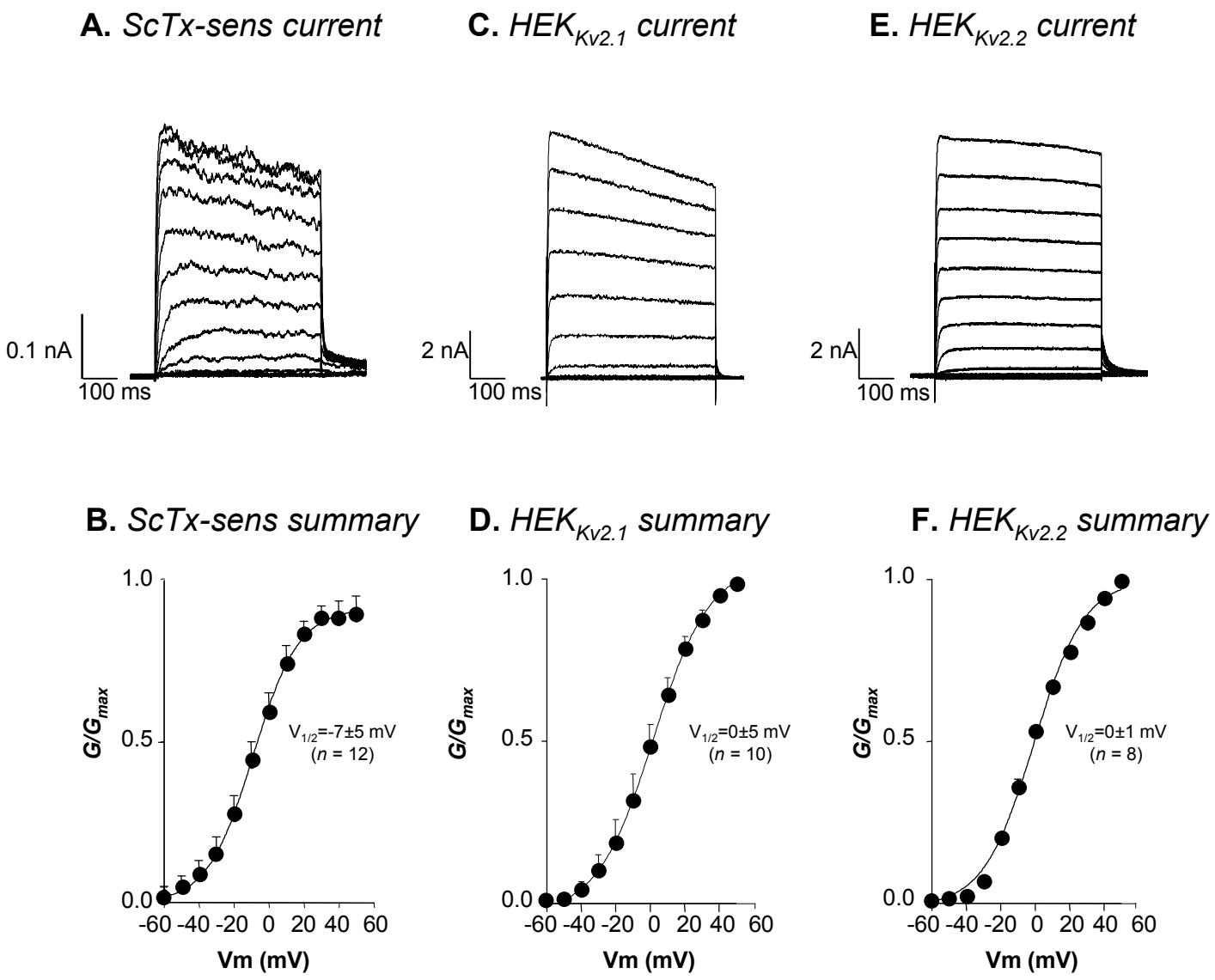
A. ScTx-sens current
C. HEK Kv2.1 current
E. HEK Kv2.2 current
0.1 nA
100 ms
2 nA
100 ms
2 nA
100 ms
B. ScTx-sens summary
D. HEK Kv2.1 summary
F. HEK Kv2.2 summary
G/Gmax
1.0
0.5
0.0
V1/2=-7±5 mV
(n = 12)
V1/2=0±5 mV
(n = 10)
V1/2=0±1 mV
(n = 8)
-60 -40 -20 0 20 40 60
Vm (mV)

Figure 6.

A: *Activation*

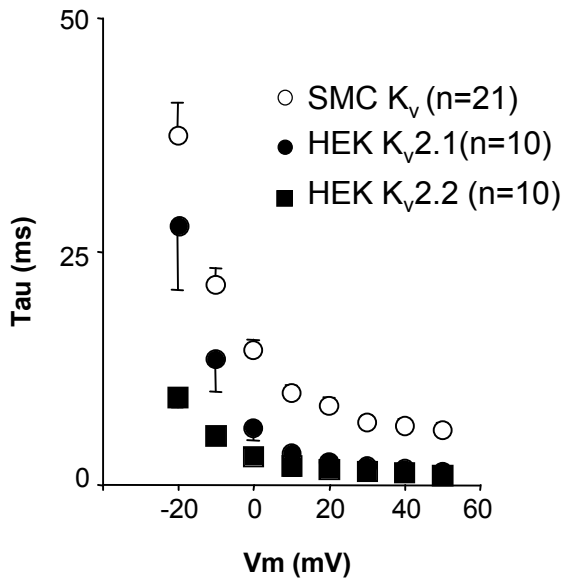

B: *Deactivation*

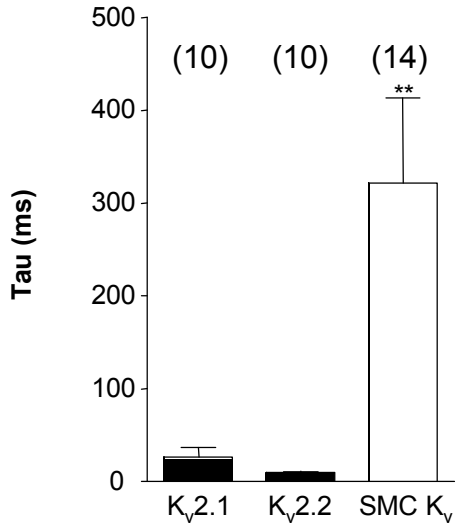

C: *Silent subunit expression*

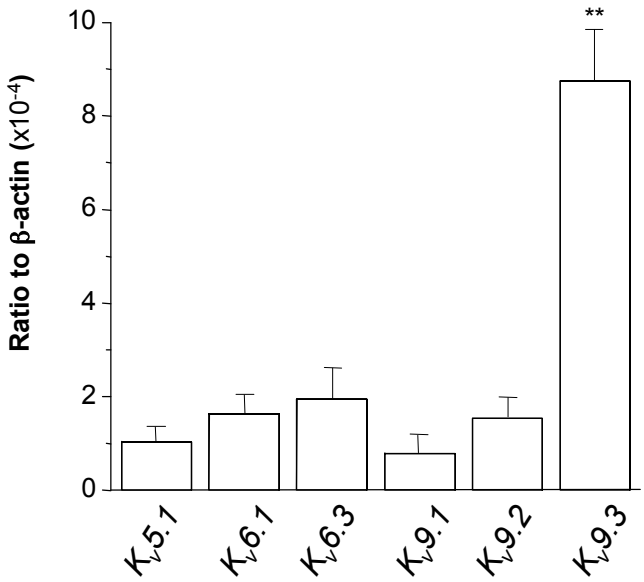

D: *K_v9.3 immunoreactivity*

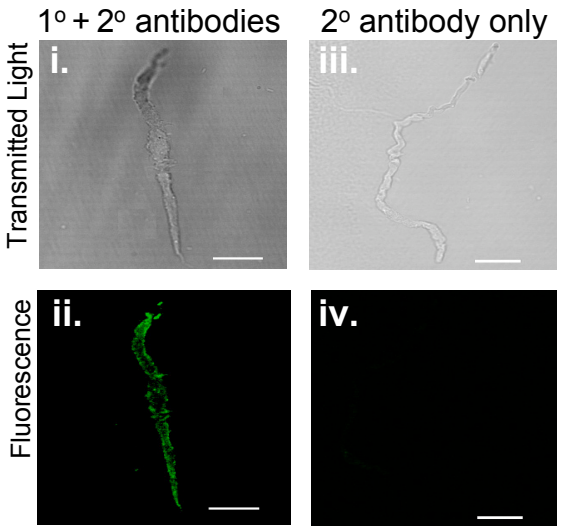

Figure 7.

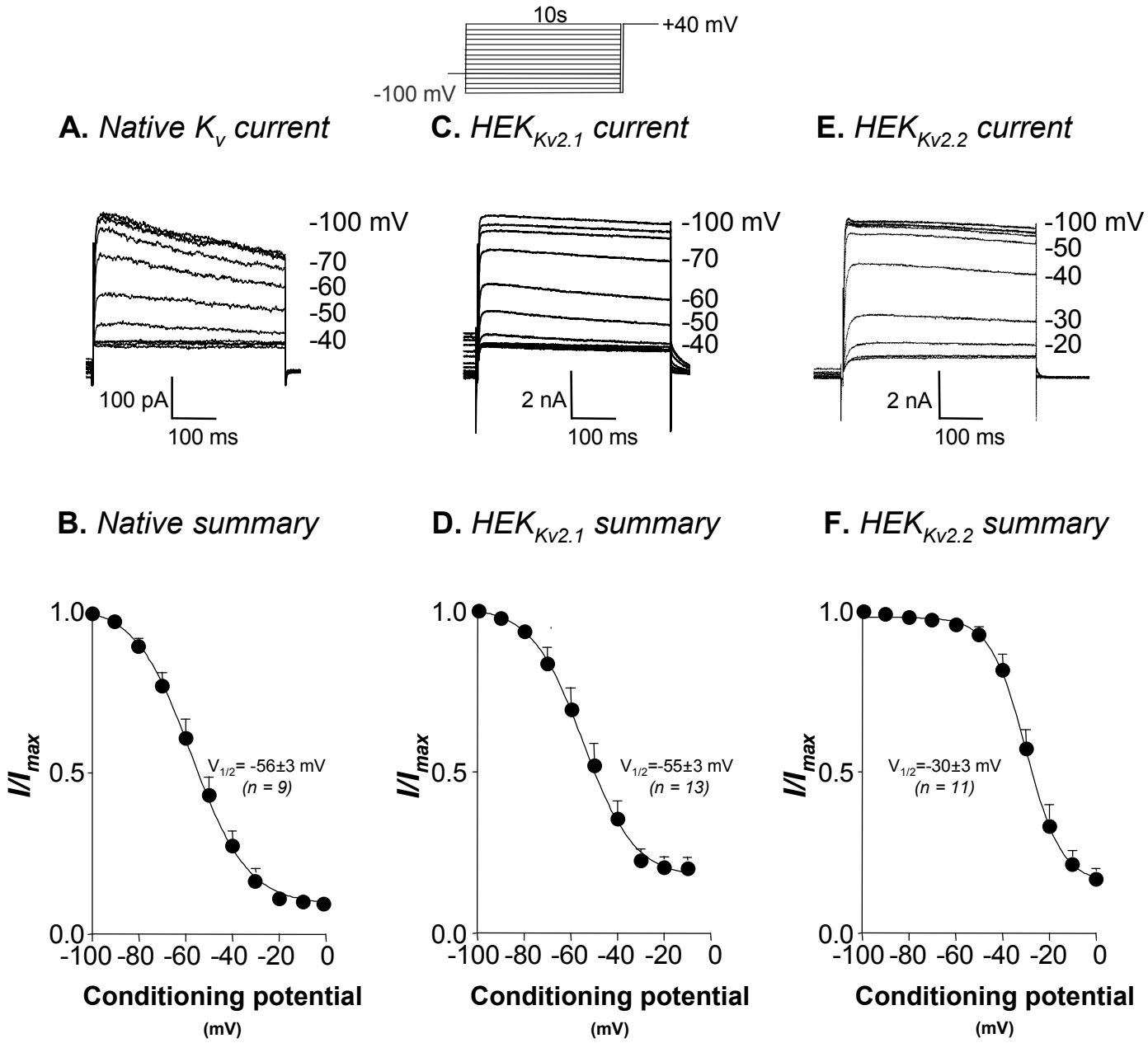
10s
+40 mV
-100 mV
A. Native K_v current
C. $HEK_{Kv2.1}$ current
E. $HEK_{Kv2.2}$ current
-100 mV
-70
-60
-50
-40
100 pA
100 ms
-100 mV
-70
-60
-50
-40
2 nA
100 ms
-100 mV
-50
-40
-30
-20
2 nA
100 ms
B. Native summary
D. $HEK_{Kv2.1}$ summary
F. $HEK_{Kv2.2}$ summary
I/I_{max}
1.0
0.5
0.0
$V_{1/2}$= -56±3 mV
(n = 9)
$V_{1/2}$=-55±3 mV
(n = 13)
$V_{1/2}$=-30±3 mV
(n = 11)
-100 -80 -60 -40 -20 0
Conditioning potential
(mV)

Figure 8.

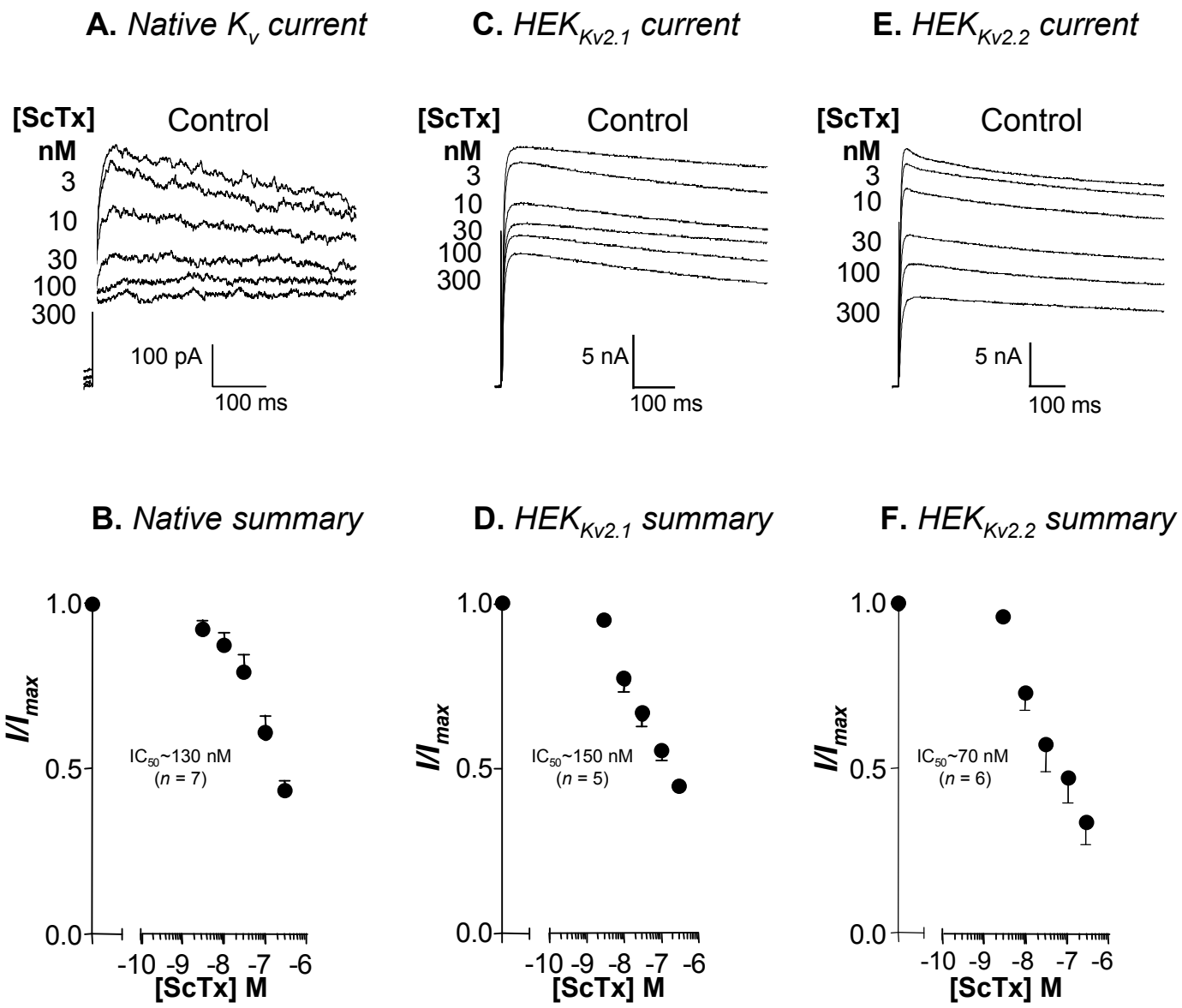
A. Native K_v current
[ScTx] nM
Control
3
10
30
100
300
100 pA
100 ms
C. $HEK_{Kv2.1}$ current
[ScTx] nM
Control
3
10
30
100
300
5 nA
100 ms
E. $HEK_{Kv2.2}$ current
[ScTx] nM
Control
3
10
30
100
300
5 nA
100 ms
B. Native summary
I/I_{max}
1.0
0.5
0.0
IC_{50}~130 nM
(n = 7)
-10 -9 -8 -7 -6
[ScTx] M
D. $HEK_{Kv2.1}$ summary
I/I_{max}
1.0
0.5
0.0
IC_{50}~150 nM
(n = 5)
-10 -9 -8 -7 -6
[ScTx] M
F. $HEK_{Kv2.2}$ summary
I/I_{max}
1.0
0.5
0.0
IC_{50}~70 nM
(n = 6)
-10 -9 -8 -7 -6
[ScTx] M

Figure 9.

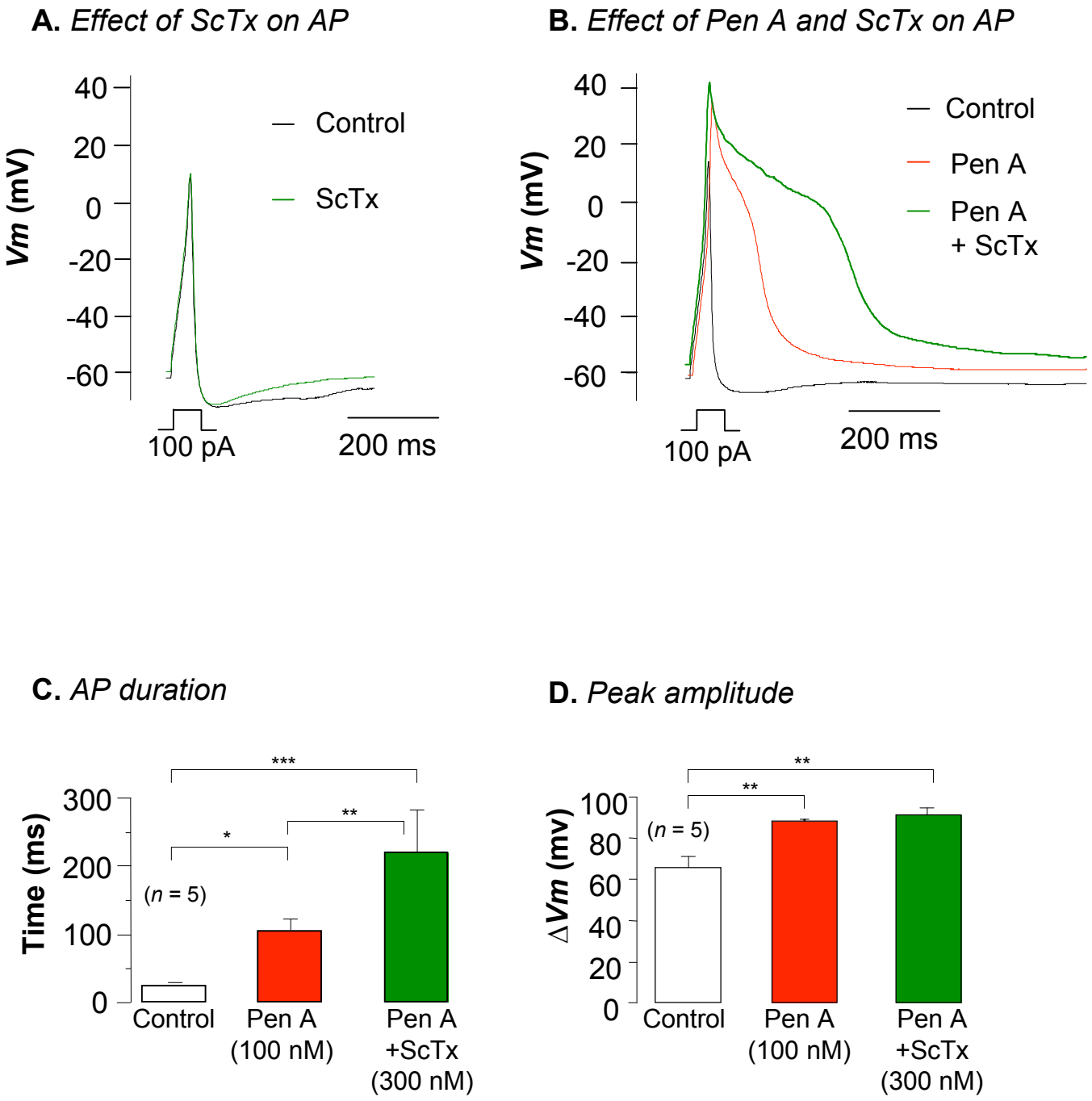
A. Effect of ScTx on AP
Vm (mV)
40
20
0
-20
-40
-60
Control
ScTx
100 pA
200 ms
B. Effect of Pen A and ScTx on AP
Vm (mV)
40
20
0
-20
-40
-60
Control
Pen A
Pen A
+ ScTx
100 pA
200 ms
C. AP duration
Time (ms)
300
200
100
0
***
**
*
(n = 5)
Control
Pen A
(100 nM)
Pen A
+ScTx
(300 nM)
D. Peak amplitude
ΔVm (mv)
100
80
60
40
20
0
**
**
(n = 5)
Control
Pen A
(100 nM)
Pen A
+ScTx
(300 nM)

Figure 10.

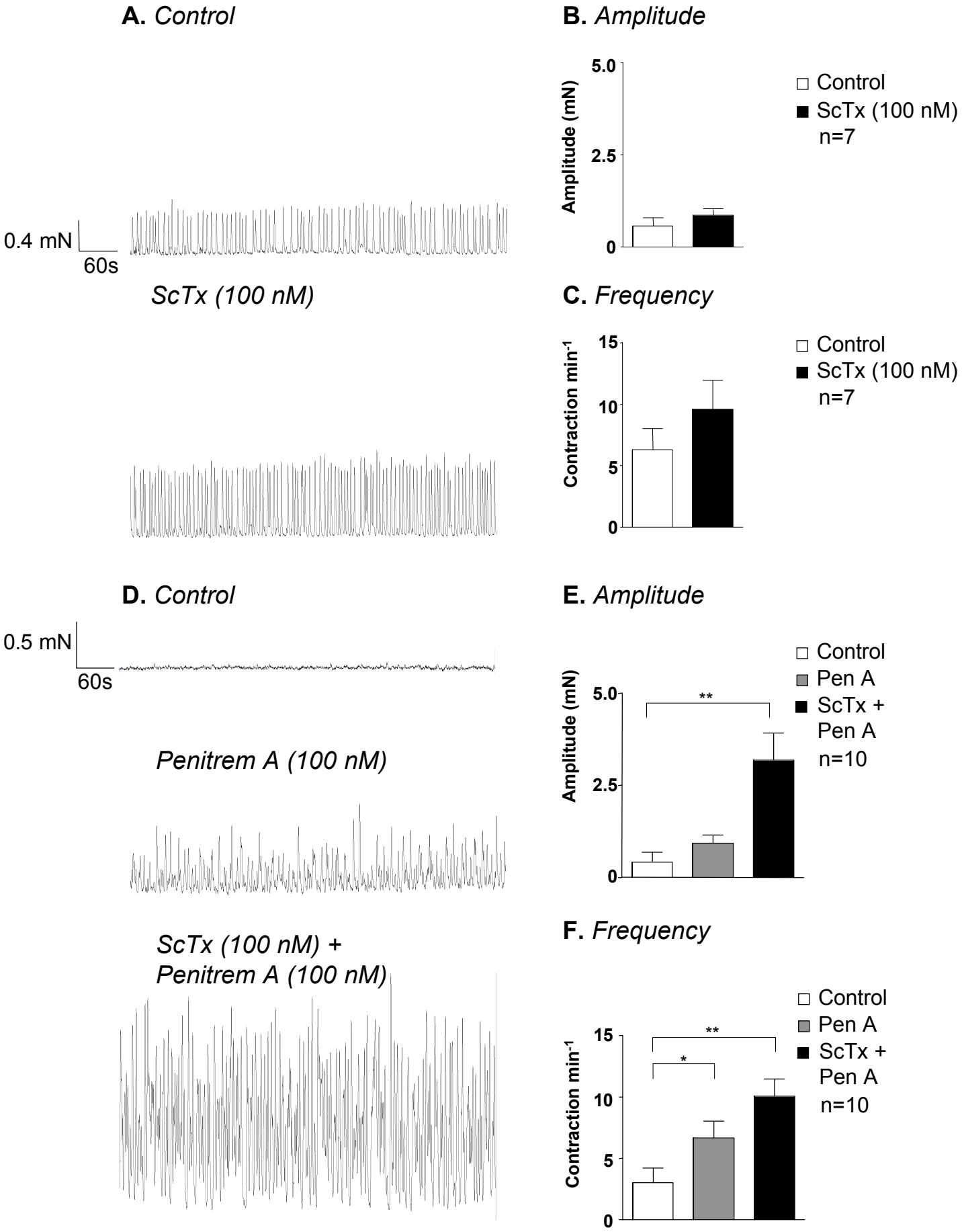
A. Control
0.4 mN
60s
ScTx (100 nM)
B. Amplitude
Amplitude (mN)
5.0
2.5
0
Control
ScTx (100 nM)
n=7
C. Frequency
Contraction min-1
15
10
5
0
Control
ScTx (100 nM)
n=7
D. Control
0.5 mN
60s
Penitrem A (100 nM)
ScTx (100 nM) +
Penitrem A (100 nM)
E. Amplitude
Amplitude (mN)
5.0
2.5
0
**
Control
Pen A
ScTx +
Pen A
n=10
F. Frequency
Contraction min-1
15
10
5
0
**
*
Control
Pen A
ScTx +
Pen A
n=10

Figure 11.